

MATERIALI A GAP INDIRETTA E TRANSIZIONI RELATIVE

4.6.1.1 Interband transitions

This recombination process is illustrated schematically on an energy level diagram for both direct and indirect bandgap materials in Figs 4.13(a) and (b) respectively. ($E-k$ diagrams for silicon and gallium arsenide are shown in Fig. 2.6.) It is important to realize that the transition must conserve the total wavevector of the system. The photon wavevector is given by $2\pi/\lambda$, whilst the electron wavevectors involved range between approximately $-\pi/a$ and

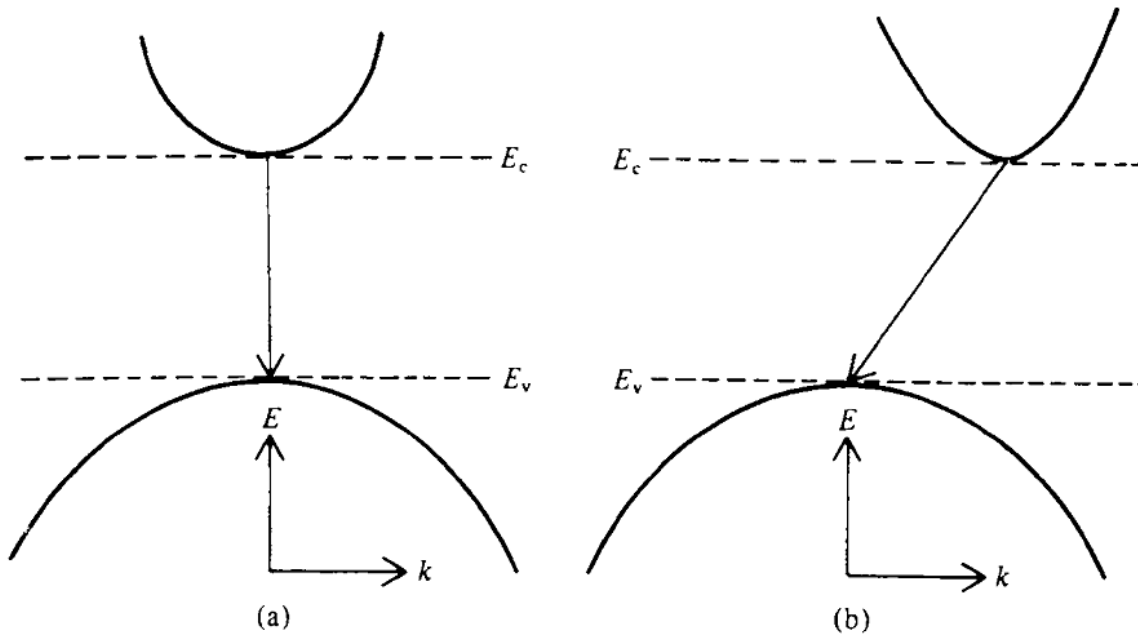


FIG. 4.13 Interband transitions for (a) a direct bandgap semiconductor and (b) for an indirect bandgap semiconductor. In the former case, there is no change in the electron k value, whilst in the latter case there is.

$+\pi/a$, where a is the crystal lattice spacing (i.e. the k values at the first Brillouin zone boundaries; see Fig. 2.5b). For visible radiation, $\lambda \approx 0.5 \times 10^{-6}$ m, whereas crystal lattice spacings are approximately 10^{-10} m; hence $2\pi/\lambda \ll \pi/a$. The photon wavevector is thus much smaller than the magnitude of the maximum possible electron wavevectors. Consequently if the only particles involved are an electron and a photon, then the electron must make a transition between states having virtually the same wavevector. On an $E-k$ diagram, therefore, only vertical transitions are allowed. It is possible to have non-vertical transitions (as illustrated in Fig. 4.13b) but to conserve the wavevector, a phonon must be either created or destroyed at the same time. The equation for the wavelength of the emitted photon is then given by

$$hc/\lambda = E_g \pm E_p \quad (4.6)$$

where E_p is the phonon energy. The + and - signs correspond to phonon *annihilation* and *creation* respectively. Phonon energies are of the order of 0.01 eV, and hence the photon wavelength in fact differs little from λ_g . However, because now *three* particles are involved

instead of just two for the direct transition process, the transition is much less probable. We know from the discussion in section 2.4 that the interband recombination rate r may be written

$$r = Bnp \quad (4.7)$$

where B is a constant. Calculated values for B in various semiconductor materials are shown in Table 4.1 (see ref. 4.7), from which we see that the values of B for indirect bandgap materials are some 10^6 times smaller than for direct bandgap materials. We conclude that band-to-band radiative transitions in indirect bandgap semiconductors are relatively rare, and unless some other radiative transition mechanisms are possible these materials will not be suitable for LEDs.

TABLE 4.1 Properties of various semiconductor materials

Group(s)	Element/ compound	Direct/ indirect	E_g (eV)	Readily doped n- or p-type	B ($m^3 s^{-1}$)	λ_g (nm)
IV	C	i	5.47			227
	Si	i	1.12	Yes	1.79×10^{-21}	1106
	Ge	i	0.67	Yes	5.25×10^{-20}	1880
IV-VI	SiC (hex. α)	i	3.00	Yes		413
III-V	AlP	i	2.45			506
	AlN	i	5.90	No		210
	AlSb	i	1.50			826
	AlAs	i	2.16			574
	GaN	d	3.40	No		365
	GaP	i	2.26	Yes	5.37×10^{-20}	549
	GaAs	d	1.43	Yes	7.21×10^{-16}	861
	InN	d	2.40			516
	InP	d	1.35	Yes	1.26×10^{-15}	918
	InAs	d	0.35		8.50×10^{-17}	3540
II-VI	InSb	d	0.18		4.58×10^{-17}	6870
	ZnO	d	3.20	No		387
	ZnS(α)	d	3.80	No		326
	ZnS(β)	d	3.60	No		344
	ZnSe	d	2.28	No		480
	ZnTe	d	2.58	No		544
	CdS	d	2.53	No		490
	CdSe	d	1.74	No		712
CdTe	d	1.50	Yes		826	

One disadvantage of radiation derived from direct bandgap recombination is that the probability of the emitted radiation being reabsorbed in band-to-band transitions can be high when the radiation has to traverse an appreciable thickness of the semiconductor material.

4.6.1.2 Impurity centre recombination

Three types of recombination involving impurity energy levels are shown in Fig. 4.14. Thus we may have (a) conduction band–acceptor level transitions, (b) donor level–valence band transitions and (c) if in addition a pair of donor and acceptor states are close together, then donor–acceptor transitions are possible. When the electron is in either type of impurity state, then it will be fairly strongly localized. This spatial localization implies that the electron can have a range of momentum values, since uncertainties in both position (Δx) and momentum (Δp) are related via the Heisenberg uncertainty relation (eq. 2.3)

$$\Delta x \Delta p \geq \hbar/2$$

Because the magnitudes of the electron wavevector k and the momentum p are related by

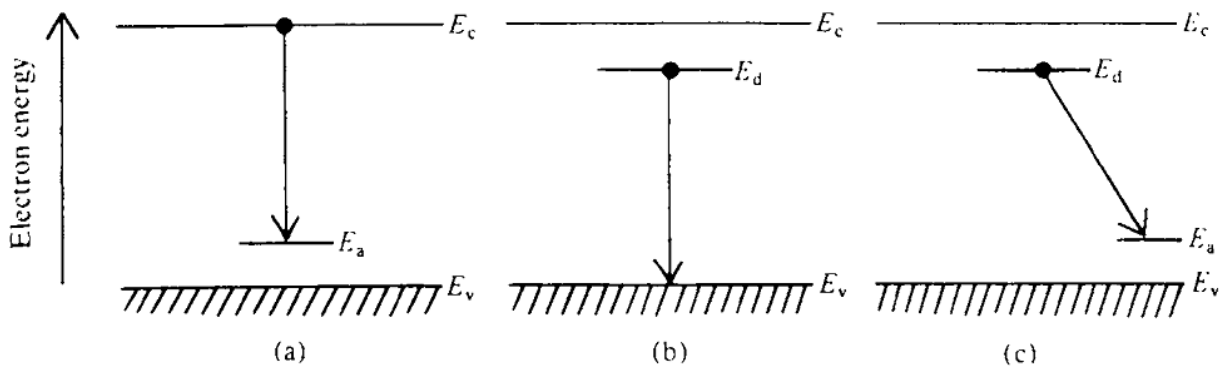


FIG. 4.14 Three types of recombination involving impurity energy levels are shown. In (a) an electron moves from the conduction band into an empty acceptor level. In (b) an electron in a donor level recombines with a hole in the valence band. In (c) an electron in a donor level falls into an empty acceptor level. This latter process requires that the donor and acceptor levels are physically close together.

$k = p/\hbar$ we may write

$$\Delta k \geq \frac{1}{2\Delta x} \quad (4.8)$$

We express the electron localization by putting $\Delta x = Na$, where a is the lattice spacing and N a number which is not expected to be much larger than unity; whence $\Delta k \geq 1/(2Na)$. In our discussion at the start of section 4.6.1.1, we noted that electrons in the conduction and valence bands have a range of k values extending approximately from $-\pi/a$ to $+\pi/a$. Hence we see that there may be sufficient spread in the k values of the impurity states to allow a significant number of transitions between them and the band extrema without calling on the assistance of phonons. Transitions via impurity states therefore provide a possible mechanism whereby indirect bandgap semiconductors can increase their radiative efficiency.

Typical values for $E_c - E_d$ and $E_a - E_v$ are of the order of 0.02 eV, so that the emission wavelength will be slightly longer than that given by eq. (4.5). However, thermal excitation within the bands themselves will tend to decrease the magnitude of this effect (see the discussion following eq. 4.5). Since the radiation has a lower photon energy than that required to excite an electron across the bandgap, it is not subject to reabsorption to the same extent as that derived from band-to-band recombinations.

Originally, LEDs were exclusively used for low-brightness applications such as indicator lamps. In these applications, the efficiency and the overall optical power of the LED are *not* of primary importance. However, in more recent applications, for example traffic light applications, the light emitted by LEDs must be seen even in bright sunlight and from a considerable distance. LEDs with high efficiency and brightness are required for such applications.

In this chapter, low-brightness as well as high-brightness LEDs are discussed. GaAsP and nitrogen-doped GaAsP LEDs are suitable only for low-brightness applications. AlGaAs LEDs are suitable for low- as well as high-brightness applications. AlGaInP and GaInN LEDs are used in high-brightness applications.

12.1 The GaAsP, GaP, GaAsP:N, and GaP:N material systems

The GaAs_{1-x}P_x and GaAs_{1-x}P_x:N material system is used for emission in the red, orange, yellow, and green wavelength range. The GaAsP system is lattice mismatched to GaAs substrates, resulting in a relatively low internal quantum efficiency. As a result these LEDs are suitable for low-brightness applications only.

GaAs_{1-x}P_x was one of the first material systems used for visible-spectrum LEDs (Holonyak and Bevacqua 1962; Holonyak *et al.* 1963, 1966; Pilkuhn and Rupprecht 1965; Wolfe *et al.*, 1965; Nuese *et al.* 1966). In the early 1960s, GaAs substrates were already available. Bulk growth of GaAs substrates was initiated in the 1950s and epitaxial growth by LPE and VPE started in the 1960s. As phosphorus is added to GaAs, the ternary alloy GaAs_{1-x}P_x, or briefly GaAsP, is formed. The addition of phosphorus increases the bandgap of GaAs, which emits in the infrared at 870 nm. The visible wavelength range starts at about 750 nm, so that a small amount of phosphorus is sufficient to attain visible-spectrum light emitters. Note, however, that the sensitivity of the human eye is low at the edges of the visible spectrum.

A significant problem with GaAsP LEDs is the lattice mismatch between the GaAs substrate

and the GaAsP epitaxial layer. A large mismatch exists between GaAs and GaP (about 3.6%) so that many misfit dislocations occur when the critical thickness of GaAsP on GaAs is exceeded. As a result, the luminescence efficiency decreases substantially in GaAsP with increasing phosphorus content. GaAsP LEDs are therefore useful for low-brightness applications only.

It was realized early in the GaAsP work that the lattice mismatch between the GaAs substrate and the GaAsP epilayer reduces the radiative efficiency. It was also found that the radiative efficiency of the active p-n junction layer strongly depends on the growth conditions and, in particular, on the thickness of the GaAsP buffer layer (Nuese *et al.*, 1969). A thick buffer layer reduces the dislocation density by annihilation of misfit dislocations. However, the dislocation density does not approach the low dislocation density of GaAs substrates, so that even with thick GaAsP buffer layers the dislocation density is substantial.

The band structure of GaAs, GaAsP, and GaP is shown schematically in Fig. 12.1. The figure shows that GaAsP is a direct-gap semiconductor for low phosphorus mole fractions. Beyond the direct–indirect crossover occurring at phosphorus mole fractions of about 45–50%, the semiconductor becomes indirect and the radiative efficiency drops rapidly (Holonyak *et al.*, 1963, 1966). GaP is an indirect-gap semiconductor and therefore is unsuitable as an efficient LED material.

GaAsP and GaP LEDs are frequently doped with isoelectronic impurities such as nitrogen (Grimmeiss and Scholz, 1964; Logan *et al.*, 1967a, 1967b, 1971; Craford *et al.*, 1972; Groves and Epstein 1977; Groves *et al.* 1978a, 1978b). The isoelectronic impurities form an optically active level within the forbidden gap of the semiconductor so that carriers recombine radiatively via the nitrogen levels, as indicated in Fig. 12.1.

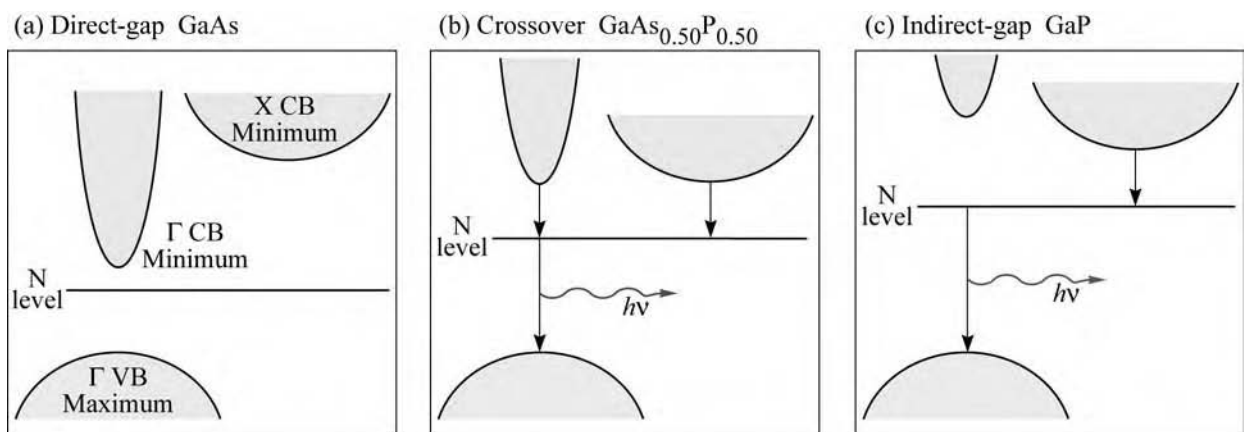


Fig. 12.1. Schematic band structure of GaAs, GaAsP, and GaP. Also shown is the nitrogen level. At a P mole fraction of 45–50%, the direct–indirect crossover occurs.

Isoelectronically doped LEDs are also interesting from a fundamental point of view. They are one of the first practical applications of Heisenberg's uncertainty principle. Isoelectronic impurities have an electronic wave function that is strongly localized in position space (small Δx). Therefore, the wave function is delocalized in momentum space (large Δp). Since the level is delocalized in momentum space, two vertical transitions can occur via the isoelectronic trap, with one of them being radiative. Physically speaking, the change in momentum, occurring when an electron makes a transition from the indirect X valley of the conduction band to the central Γ valley of the valence band, is absorbed by the isoelectronic impurity atom.

The emission wavelength of undoped and nitrogen-doped GaAsP is shown in Fig. 12.2 (Craford *et al.*, 1972). The emission energy of GaAsP and GaP doped with the isoelectronic impurity nitrogen is below the bandgap of the semiconductor. Figure 12.2 illustrates that the emission energy is about 50–150 meV below the bandgap of the semiconductor. As a result, reabsorption effects are much less likely in nitrogen-doped structures compared with LEDs based on band-edge emission. This is a substantial advantage of LEDs doped with isoelectronic impurities.

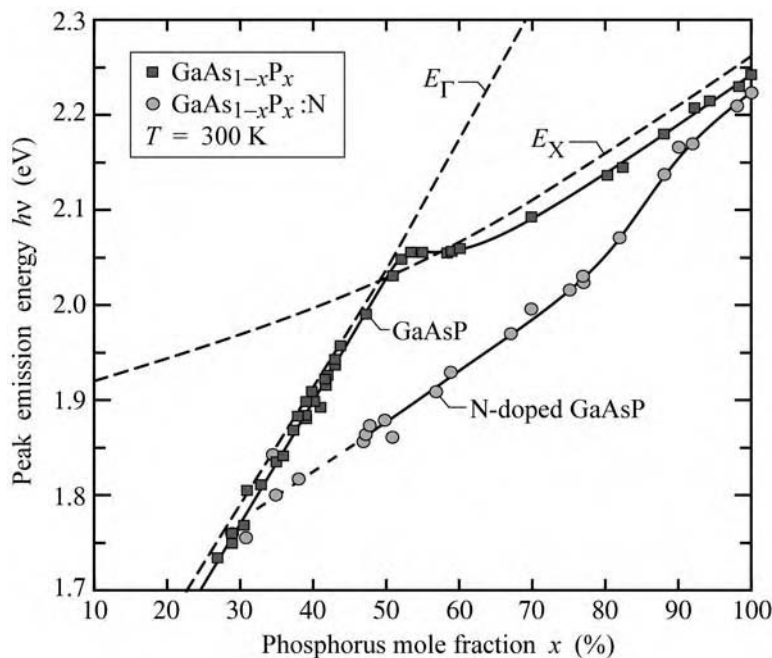


Fig. 12.2. Room-temperature peak emission energy versus alloy composition for undoped and nitrogen-doped GaAsP LEDs injected with a current density of 5 A/cm^2 . Also shown is the energy gap of the direct-to-indirect (E_{Γ} -to- E_X) transition. The direct-indirect crossover occurs at $x \approx 50\%$ (after Craford *et al.*, 1972).

Groves *et al.* (1978a, 1978b) showed that this advantage is particularly pronounced if only the active region is doped with nitrogen. In this case, the region of the p-n junction plane and the regions located within the carrier diffusion lengths from the junction plane are doped with nitrogen. Other regions, such as the confinement and window layers, are not doped with the

isoelectronic impurity, so that reabsorption of light by the isoelectronic impurities is limited to the narrow active region. Quantum efficiencies of several percent can be attained with GaP:N LEDs in which the nitrogen doping is limited to the active region.

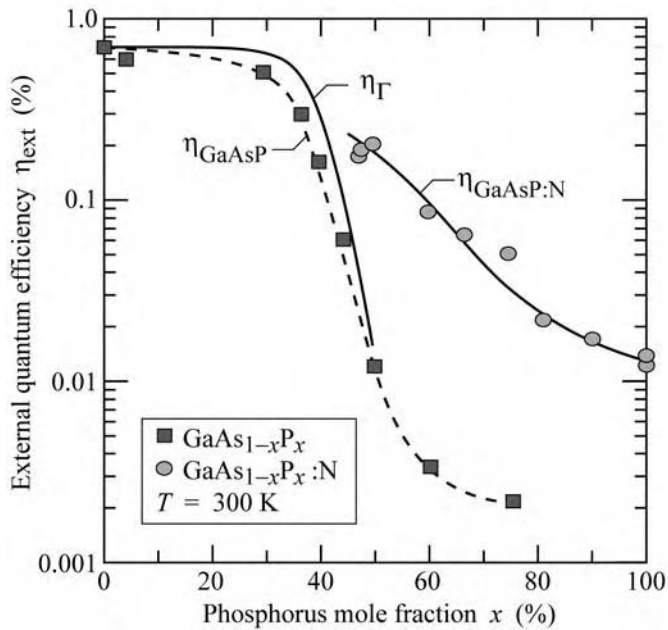


Fig. 12.3. Experimental external quantum efficiency of undoped and N-doped GaAsP versus the P mole fraction. Also shown is the calculated direct-gap (Γ) transition efficiency, η_{Γ} , and the calculated nitrogen (N) related transition efficiency, η_{N} (solid lines). Note that the nitrogen-related efficiency is higher than the direct-gap efficiency in the indirect bandgap ($x > 50\%$) regime (after Campbell *et al.*, 1974).

The external quantum efficiency of undoped and nitrogen-doped GaAsP is shown in Fig. 12.3 (Campbell, 1974). Only the vicinity of the active region is doped with nitrogen. The efficiency of the nitrogen-doped LEDs is strongly enhanced over the entire composition range compared with the GaAsP LEDs without nitrogen doping.

Note that the GaAsP LED efficiency decreases by more than two orders of magnitude in the composition range $x = 40\text{--}60\%$. This decrease is due to the direct–indirect crossover occurring in GaAsP and due to the increasing dislocation density occurring at higher phosphorus mole fractions. At a phosphorus mole fraction of 75%, the GaAsP external quantum efficiency is only 0.002%.

The external quantum efficiency of undoped and nitrogen-doped GaAsP versus emission wavelength is shown in Fig. 12.4. Again, only the vicinity of the active region is doped with nitrogen. The efficiency of nitrogen-doped GaAsP is higher than that of undoped GaAsP, in particular in the orange, yellow, and green wavelength range where the improvement is a factor of 2–5. In the red wavelength range, the undoped and nitrogen-doped GaAsP LEDs have similar efficiencies.

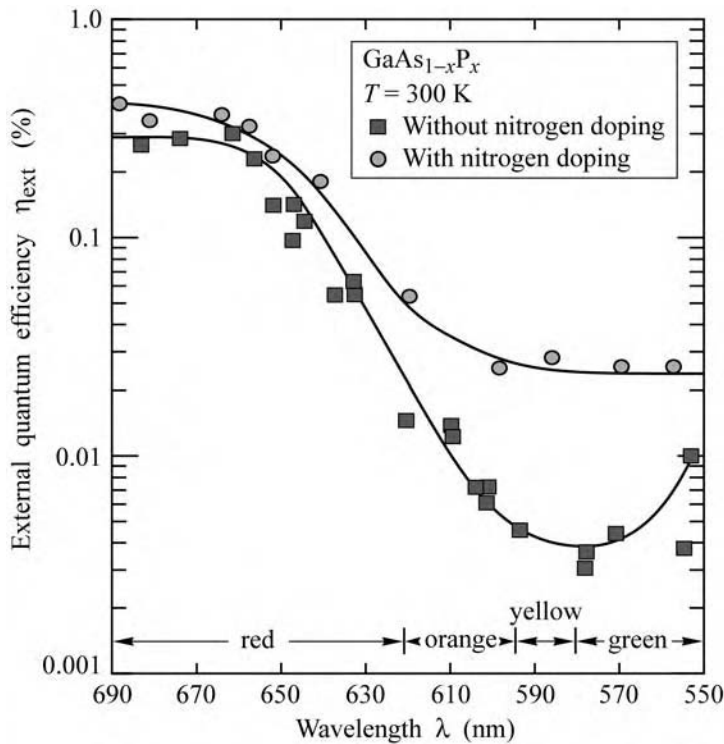


Fig. 12.4. External quantum efficiency versus emission wavelength in undoped and nitrogen-doped $\text{GaAs}_{1-x}\text{P}_x$ (after Groves *et al.*, 1978a, 1978b).

The ratio of external quantum efficiencies of undoped and nitrogen-doped GaAsP LEDs is shown in Fig. 12.5. It is inferred from the figure that nitrogen-doped devices have a higher efficiency over the entire composition range.

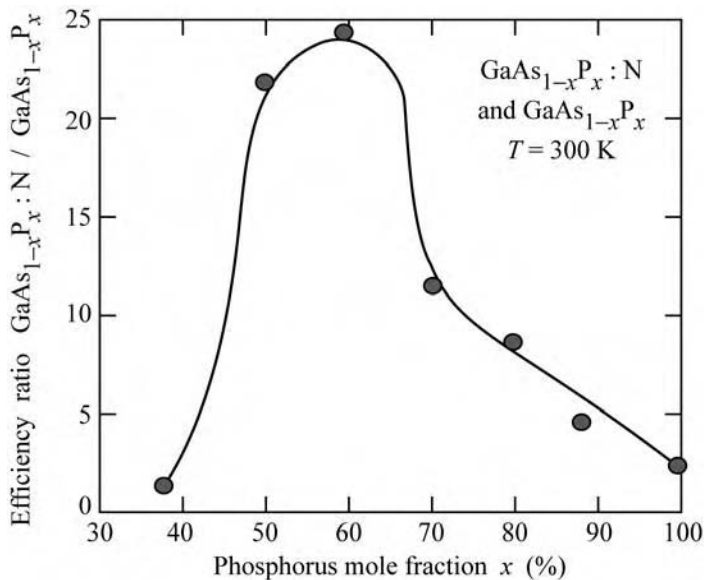


Fig. 12.5. Efficiency ratio between nitrogen-doped and undoped $\text{GaAs}_{1-x}\text{P}_x$ at 300 K (after Groves *et al.*, 1978a, 1978b).

The brightness of LEDs based on isoelectronic impurity transitions is limited by the *finite solubility* of nitrogen. For example, nitrogen is soluble in GaP up to nitrogen concentrations of

about 10^{20} cm^{-3} . Since an optical transition via a nitrogen level has a certain lifetime, the maximum nitrogen concentration limits the LED operation to a maximum current beyond which the LED efficiency decreases.

Commercial low-brightness green LEDs are based on nitrogen-doped GaP. The main application of GaP:N LEDs is indicator lamps. However, nitrogen-doped GaP LEDs are not suitable for high-brightness applications, i.e. for applications under bright ambient light conditions such as sunlight. High-brightness green LEDs are based on GaInN.

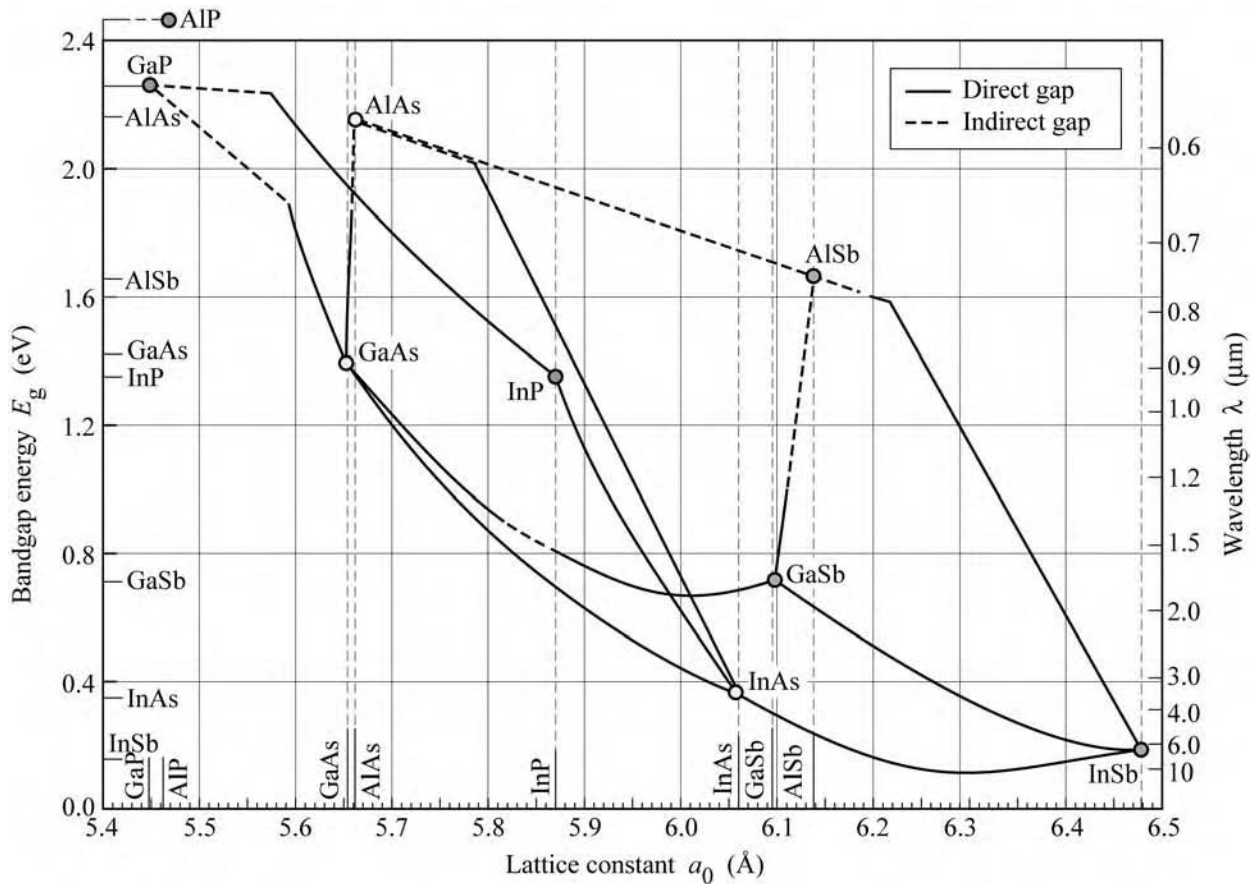


Fig. 12.6. Bandgap energy and lattice constant of various III–V semiconductors at room temperature (after Tien, 1988).

12.2 The AlGaAs/GaAs material system

The $\text{Al}_x\text{Ga}_{1-x}\text{As}/\text{GaAs}$ material system was developed in the 1970s and early 1980s and it was the first material system suitable for high-brightness LED applications (for a review, see Steranka, 1997). Owing to the very similar atomic radii of Al (1.82 Å) and Ga (1.81 Å), the material system $\text{Al}_x\text{Ga}_{1-x}\text{As}$ (or briefly AlGaAs) is lattice matched to GaAs for all Al mole

fractions. The lack of dependence of the lattice constant on the Al mole fraction can be inferred from Fig. 12.6, which shows the energy gap and lattice constant of several III–V semiconductors and of its ternary and quaternary alloys as a function of the lattice constant (adopted from Tien, 1988).

GaAs and $\text{Al}_x\text{Ga}_{1-x}\text{As}$ for Al mole fractions $x < 0.45$ are direct-gap semiconductors. The energy gap of $\text{Al}_x\text{Ga}_{1-x}\text{As}$ versus the Al mole fraction is shown in Fig. 12.7 (Casey and Panish, 1978). For Al mole fractions $x < 45\%$, the Γ conduction-band valley is the *lowest* minimum and the semiconductor has a *direct* gap. For $x > 45\%$, the X valleys are the *lowest* conduction-band minimum and the semiconductor becomes *indirect*.

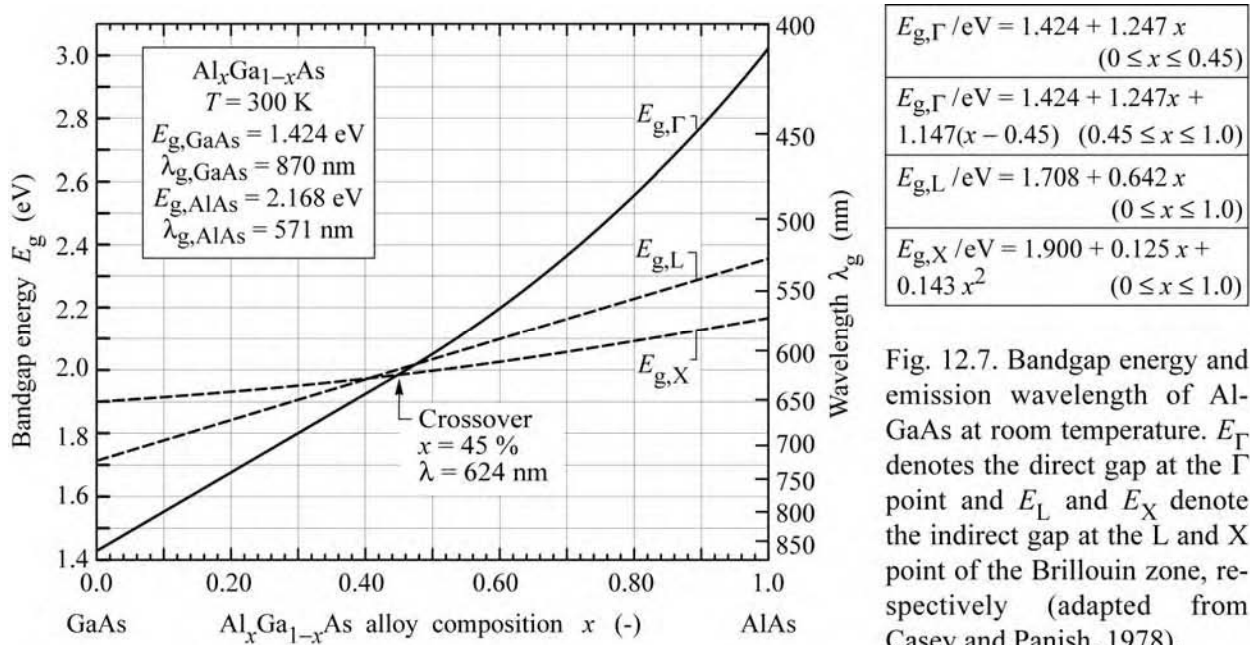


Fig. 12.7. Bandgap energy and emission wavelength of AlGaAs at room temperature. E_{Γ} denotes the direct gap at the Γ point and E_L and E_X denote the indirect gap at the L and X point of the Brillouin zone, respectively (adapted from Casey and Panish, 1978).

The AlGaAs material system is suited for high-brightness visible-spectrum LEDs emitting in the red wavelength range. The direct–indirect crossover occurs at a wavelength of 621 nm. At that wavelength, the radiative efficiency of the AlGaAs system becomes quite low due to the direct–indirect transition. To maintain high efficiency, the emission energy must be several kT lower than the bandgap energy at the direct–indirect crossover point.

There are several possible strategies for AlGaAs-based red LEDs, including $\text{Al}_x\text{Ga}_{1-x}\text{As}$ bulk active regions, $\text{Al}_x\text{Ga}_{1-x}\text{As}/\text{GaAs}$ quantum well active regions, and $\text{Al}_x\text{Ga}_{1-x}\text{As}/\text{Al}_y\text{Ga}_{1-y}\text{As}$ ($x > y$) double heterostructure active regions. The first possibility, $\text{Al}_x\text{Ga}_{1-x}\text{As}$ bulk active regions, lacks the advantages of a heterostructure and this approach is therefore not used in high-brightness LEDs. The two other possibilities are more attractive due to the employment of

heterostructures. The quantum well and double heterostructure active region is used in high-efficiency red LEDs and the two structures are shown schematically in Fig. 12.8. In the $\text{Al}_x\text{Ga}_{1-x}\text{As}/\text{GaAs}$ quantum well case shown in Fig. 12.8 (a), size quantization is used to increase the emission energy. In the case of the $\text{Al}_x\text{Ga}_{1-x}\text{As}/\text{Al}_y\text{Ga}_{1-y}\text{As}$ double heterostructures shown in Fig. 12.8 (b), AlGaAs is used for both the barrier region and the well region. A drawback of the $\text{Al}_x\text{Ga}_{1-x}\text{As}/\text{GaAs}$ quantum well active regions is the requirement of very thin GaAs quantum wells clad by $\text{Al}_x\text{Ga}_{1-x}\text{As}$ barriers. Vertical transport in multi-quantum well (MQW) structures can lead to non-uniform carrier distribution in the MQW active region unless the barriers are very thin. Consequently, the $\text{Al}_x\text{Ga}_{1-x}\text{As}/\text{Al}_y\text{Ga}_{1-y}\text{As}$ double heterostructure approach is usually preferred.

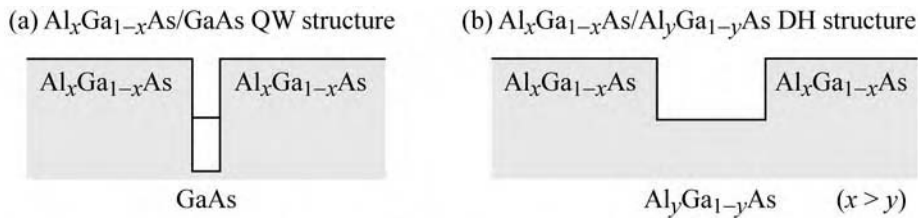


Fig. 12.8. Band diagrams of AlGaAs/GaAs structures suited for emission in the red part of the visible spectrum. (a) AlGaAs/GaAs quantum well (QW) structure with a thin GaAs well. (b) AlGaAs/AlGaAs double heterostructure (DH) with an AlGaAs active region.

AlGaAs/GaAs LEDs have been fabricated as homostructures, single heterostructures, and double heterostructures (Nishizawa *et al.*, 1983). The most efficient AlGaAs red LEDs are double-heterostructure transparent-substrate (DH-TS) devices (Ishiguro *et al.*, 1983; Steranka *et al.* 1988; Ishimatsu and Okuno, 1989). **AlGaAs DH-TS LEDs** are grown on temporary GaAs substrates and consist of a thick (e.g. 125 μm) $\text{Al}_x\text{Ga}_{1-x}\text{As}$ lower confinement layer with an Al mole fraction $x > 60\%$, an $\text{Al}_x\text{Ga}_{1-x}\text{As}$ active layer ($x = 35\%$, for red devices), and a thick (e.g. 125 μm) $\text{Al}_x\text{Ga}_{1-x}\text{As}$ upper confinement layer, also with an Al mole fraction $x > 60\%$. For devices emitting in the IR, the Al mole fractions of the active and confinement layers can be lower. After epitaxial growth, the absorbing GaAs substrate is removed by polishing and selective wet chemical etching. AlGaAs DH-TS LEDs are more than a factor of 2 brighter than double-heterostructure absorbing-substrate (DH-AS) devices (Steranka *et al.*, 1988).

In the 1980s the growth method of choice for AlGaAs DH-TS LEDs was liquid-phase epitaxy (LPE). This growth method is capable of growing, at a high growth rate, very thick high-quality AlGaAs layers with high Al content. LPE can be scaled up for high-volume production

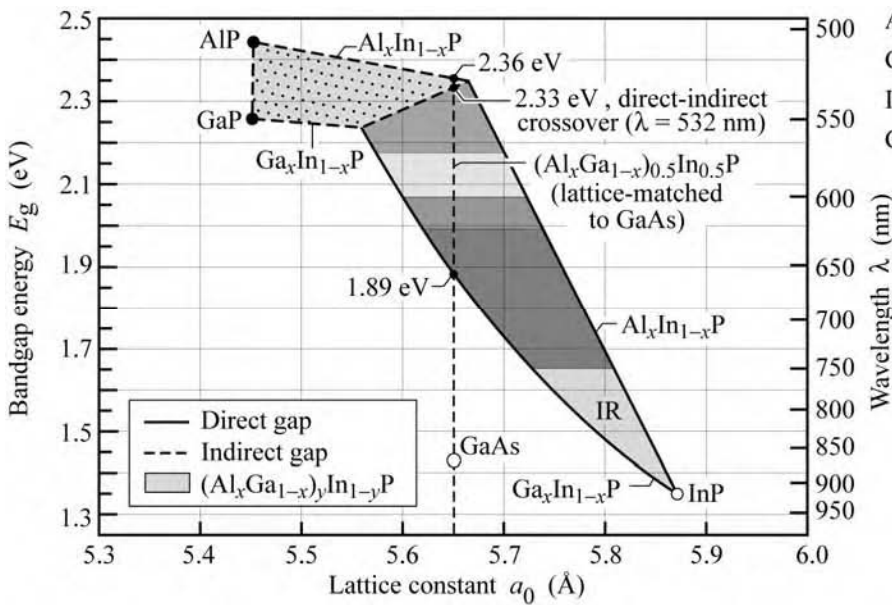
(Ishiguro *et al.*, 1983; Steranka *et al.*, 1988; Ishimatsu and Okuno, 1989). AlGaAs/GaAs DH-AS LEDs have also been grown by OMVPE (Bradley *et al.*, 1986). However, the OMVPE growth rate is lower than the LPE growth rate. OMVPE growth of thick layers, as required for DH-TS devices, is therefore difficult. Historically AlGaAs DH-TS LEDs were the first high-brightness LEDs suitable for demanding applications such as automotive brake lights and traffic lights, which must be clearly visible under bright ambient conditions.

The reliability of AlGaAs devices is known to be lower than that of AlGaInP devices that do not contain any AlGaAs. High-Al-content AlGaAs layers are subject to oxidation and corrosion, thereby lowering the device lifetime. Dallesasse *et al.* (1990) reported the deterioration of AlGaAs/GaAs heterostructures by hydrolysis. Cracks, fissures, and pinholes were found after long-term exposure to room environmental conditions, especially for thick AlGaAs layers ($> 0.1 \mu\text{m}$) with a high Al content such as 85%. The authors found very thin AlGaAs layers (e.g. 20 nm) to be stable, even for Al contents of 100%. Hermetic packaging is required to avoid oxidation and hydrolysis of AlGaAs layers. Steranka *et al.* (1988) stated that some AlGaAs devices on the market have exhibited severe degradation. However, accelerated aging data taken at 55 °C with an injection current of 30 mA showed no degradation at all after 1000 h of stress. Such a performance requires excellent understanding and control of the device fabrication and packaging process.

12.3 The AlGaInP/GaAs material system

The AlGaInP material system was developed in the late 1980s and early 1990s and today is the primary material system for high-brightness LEDs emitting in the long-wavelength part of the visible spectrum, i.e. in the red, orange, amber, and yellow wavelength range. The AlGaInP material system and AlGaInP LEDs have been reviewed by Stringfellow and Craford (1997), Chen *et al.* (1997), and Kish and Fletcher (1997). Further reviews and recent developments were published by Mueller (1999, 2000) and Krames *et al.* (2002).

Figure 12.9 shows the energy gap and the corresponding wavelength versus the lattice constant of AlGaInP (Chen *et al.*, 1997). AlGaInP can be lattice matched to GaAs. Replacing all As atoms in the GaAs lattice by *smaller* P atoms and some of the Ga atoms in the GaAs lattice by *larger* In atoms, forms GaInP, which at the particular composition $\text{Ga}_{0.5}\text{In}_{0.5}\text{P}$, is lattice matched to GaAs. Since Al and Ga have very similar atomic radii, the material $(\text{Al}_x\text{Ga}_{1-x})_{0.5}\text{In}_{0.5}\text{P}$ is also lattice matched to GaAs.



AlP: $E_g = 2.45$ eV, $a_0 = 5.4510$ Å
 GaP: $E_g = 2.26$ eV, $a_0 = 5.4512$ Å
 InP: $E_g = 1.35$ eV, $a_0 = 5.8686$ Å
 GaAs: $E_g = 1.424$ eV, $a_0 = 5.6533$ Å

Fig. 12.9. Bandgap energy and corresponding wavelength versus lattice constant of $(Al_xGa_{1-x})_yIn_{1-y}P$ at 300 K. The vertical dashed line shows $(Al_xGa_{1-x})_{0.5}In_{0.5}P$ lattice matched to GaAs (adapted from Chen *et al.*, 1997).

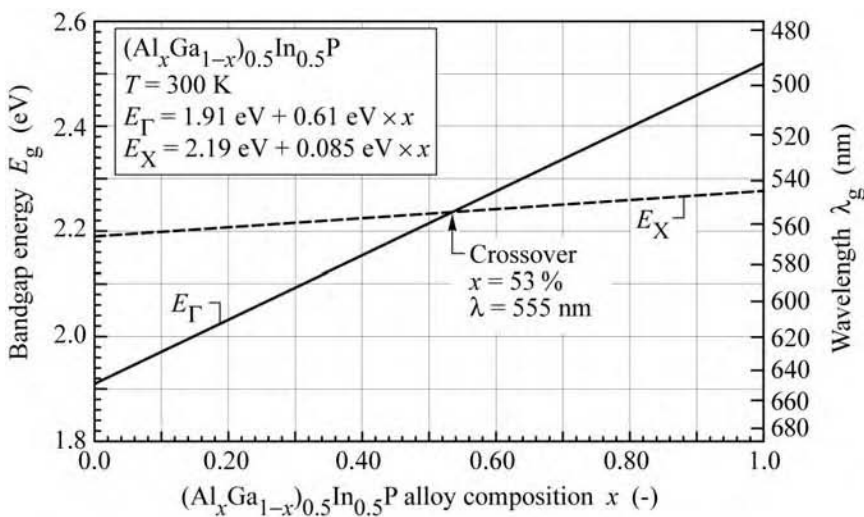


Fig. 12.10. Bandgap energy and emission wavelength of unordered AlGaInP lattice matched to GaAs at room temperature. E_Γ denotes the direct gap at the Γ point and E_X denotes the indirect gap at the X point of the Brillouin zone (after Prins *et al.*, 1995 and Kish and Fletcher, 1997).

According to Chen *et al.* (1997), $(Al_xGa_{1-x})_{0.5}In_{0.5}P$ has a direct bandgap for $x < 0.5$ and an indirect bandgap for $x > 0.5$. At the crossover point ($x = 0.5$), the bandgap energy is 2.33 eV, corresponding to a wavelength of 532 nm. Kish and Fletcher (1997) compiled data from Prins *et al.* (1995) and concluded that $(Al_xGa_{1-x})_{0.5}In_{0.5}P$ is a direct-gap semiconductor for Al mole fractions $x < 0.53$. The energy gap versus Al mole fraction is shown in Fig. 12.10 (Prins *et al.*, 1995; Kish and Fletcher, 1997). At Al mole fractions $x < 53\%$, the Γ conduction-band valley is the lowest minimum and the semiconductor has a direct gap. For $x > 53\%$, the X valleys are the lowest conduction-band minimum and the semiconductor becomes indirect. The emission wavelength at the direct–indirect crossover point is approximately 555 nm. The exact

wavelength of the crossover point may depend on the degree of atomic ordering present in a particular material (Kish and Fletcher, 1997).

A contour plot of the lattice constant and the energy gap of the AlGaInP materials system is shown in Fig. 12.11 (Chen *et al.*, 1997). The bandgap energy values and the composition of the direct–indirect crossover shown in Fig. 12.11 are slightly different from the data shown in Fig. 12.10, which can be attributed to atomic ordering in AlGaInP. Atomic ordering lowers the bandgap energy by values up to 190 meV (Kish and Fletcher, 1997).

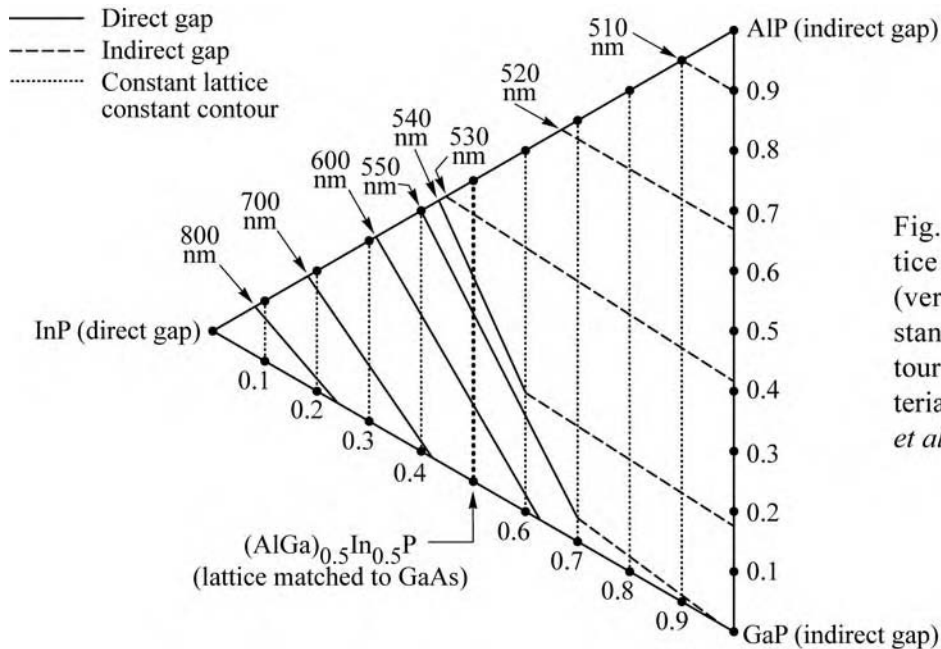


Fig. 12.11. Constant lattice constant contours (vertical lines) and constant emission line contours of the AlGaInP materials system (after Chen *et al.*, 1997).

The AlGaInP material system is suited for high-brightness visible-spectrum LEDs emitting in the red, orange, amber, and yellow wavelength range. At the direct–indirect crossover the radiative efficiency of the AlGaInP system is quite low due to the direct–indirect transition. To maintain high efficiency, the emission energy should be several kT lower than the bandgap energy at the direct–indirect crossover point.

12.4 The GaInN material system

The GaInN material system was developed in the early 1990s. GaInN LEDs emitting in the blue and green wavelength range became commercially available in the late 1990s. To date GaInN is the primary material system for high-brightness blue and green LEDs. The GaInN material system and GaInN LEDs have been reviewed by Nakamura and Fasol (1997) and by Strite and Morkoc (1992).

One of the greatest surprises of the GaInN materials system is its high radiative efficiency despite the presence of a very high concentration of threading dislocations in GaInN/GaN epitaxial films. These threading dislocations are due to the lattice mismatch between the commonly used sapphire and SiC substrates and the GaN and GaInN epitaxial films. Typical densities of the threading dislocations are in the 10^7 – 10^9 cm^{-2} range.

In the III–V arsenide and III–V phosphide material systems, misfit dislocations have disastrous consequences for the radiative efficiency. The lack of such strongly detrimental consequences in the GaInN material system is not fully understood. However, it is believed that the small diffusion length of holes and an apparently low electrical activity of dislocations in GaN and GaInN allows for high radiative efficiencies.

It has also been postulated that fluctuations of the In content in GaInN cause carriers to be localized in potential minima, thus preventing carriers from reaching dislocations. The carriers localized in potential minima will eventually recombine radiatively. Although the physical mechanisms of the high radiative efficiency of GaInN are not yet understood in detail, it is clear that the optical properties of III–V nitrides are much less affected by dislocations than those of III–V arsenides and III–V phosphides.

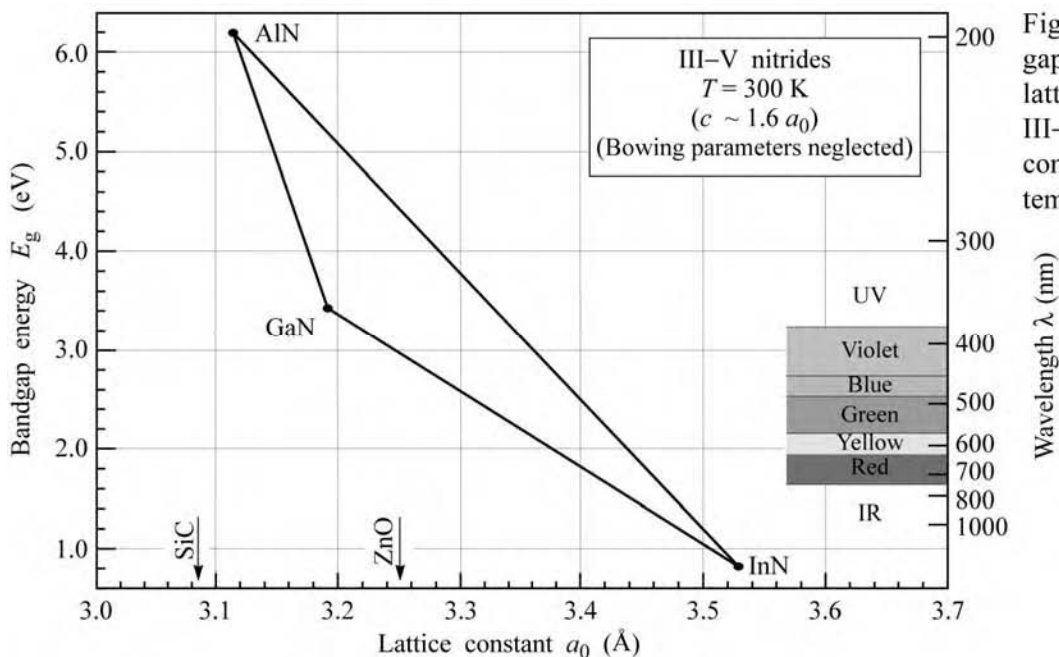
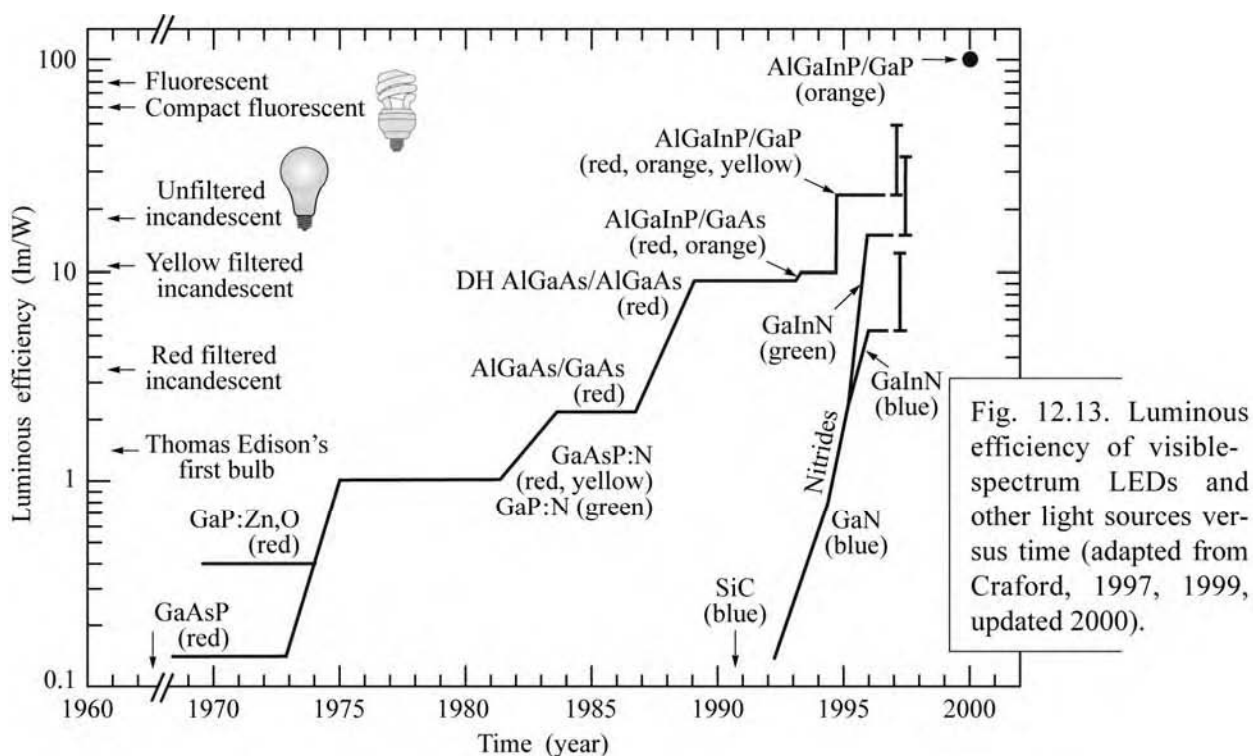


Fig. 12.12. Bandgap energy versus lattice constant of III–V nitride semiconductors at room temperature.

The bandgap energy versus the lattice constant in the nitride material family is shown in Fig. 12.12. Inspection of the figure indicates that GaInN is, in theory, suitable for covering the entire visible spectrum. However, the growth of high-quality GaInN becomes increasingly more

difficult as the In composition is increased, in part due to re-evaporation of In from the growth surface. As a result, the GaInN material system is exclusively used for ultraviolet (UV), blue, and green LEDs at the present time and rarely for longer wavelengths.

Prior to the year 2002, the generally accepted value for the InN bandgap energy was 1.9 eV. However, Wu *et al.* (2002a, 2002b) showed by luminescence measurements that the bandgap of InN is lower, namely between 0.7 and 0.8 eV. Luminescence measurements also indicated that the InN bandgap exhibits an unusual blue shift with increasing temperature.



12.5 General characteristics of high-brightness LEDs

The improvement in luminous efficiency of visible-spectrum LEDs has been truly breathtaking. The advancement of LED efficiency can be compared to the advancement made in Si integrated circuits where the performance increase versus time has been characterized by “Moore’s law”. This “law” states that the performance of Si integrated circuits doubles approximately every 18 months.

The historical development of the luminous efficiency of visible-spectrum LEDs is shown in Fig. 12.13 (Craford, 1997, 1999). The chart illustrates the modest beginnings of visible-spectrum LED technology which started in the 1960s. If the progress from 1960 to 2000 is assumed to be

continuous, then the LED luminous efficiency has doubled every 4 years. The following types of LEDs are shown in the figure.

- GaAsP LEDs grown on GaAs substrates. The GaAsP/GaAs material system is lattice mismatched so that an abundance of misfit dislocations occurs in GaAsP epitaxial films. As a result, these LEDs have a low luminous efficiency (of the order of only 0.1 lm/W). Red GaAsP LEDs are still being manufactured due to the simple epitaxial growth and low fabrication cost.
- GaP LEDs doped with radiative recombination centers. Pure GaP is an indirect semiconductor and therefore has a low radiative efficiency. However, when doped with isoelectronic impurities such as N or co-doped with Zn and O, radiative transitions in the red and green spectral range occur via these centers.
- GaAsP/GaAs LEDs doped with N emitting in the red. Again a mismatched materials system with low efficiency due to the abundance of misfit dislocations.
- AlGaAs/GaAs LEDs emitting in the red. These LEDs employ GaAs quantum well active regions.
- AlGaAs/AlGaAs double heterostructure LEDs emitting in the red using AlGaAs active regions and AlGaAs barriers.
- AlGaInP/GaAs LEDs with absorbing GaAs substrates
- AlGaInP/GaP LEDs and with wafer-bonded transparent GaP substrates.
- Also included in the chart is a result by Krames *et al.* (1999) who reported LEDs with efficiencies exceeding 100 lm/W using AlGaInP/GaP LEDs with truncated inverted-pyramid-shaped dies.
- GaInN LEDs emitting in the blue and green wavelength range.

Figure 12.13 also shows the luminous efficiency of conventional light sources including Edison's first light bulb (1.4 lm/W) and red and yellow filtered incandescent lamps. Inspection of the figure reveals that LEDs outperform filtered red and yellow incandescent lights by a large margin.

The luminous efficiency of high-brightness LEDs and of some low-cost LEDs is shown versus wavelength in Fig. 12.14 (United Epitaxy Corp., 1999). The figure indicates that yellow (590 nm) and orange (605 nm) AlGaInP and green (525 nm) GaInN LEDs are excellent choices for high luminous efficiency devices.

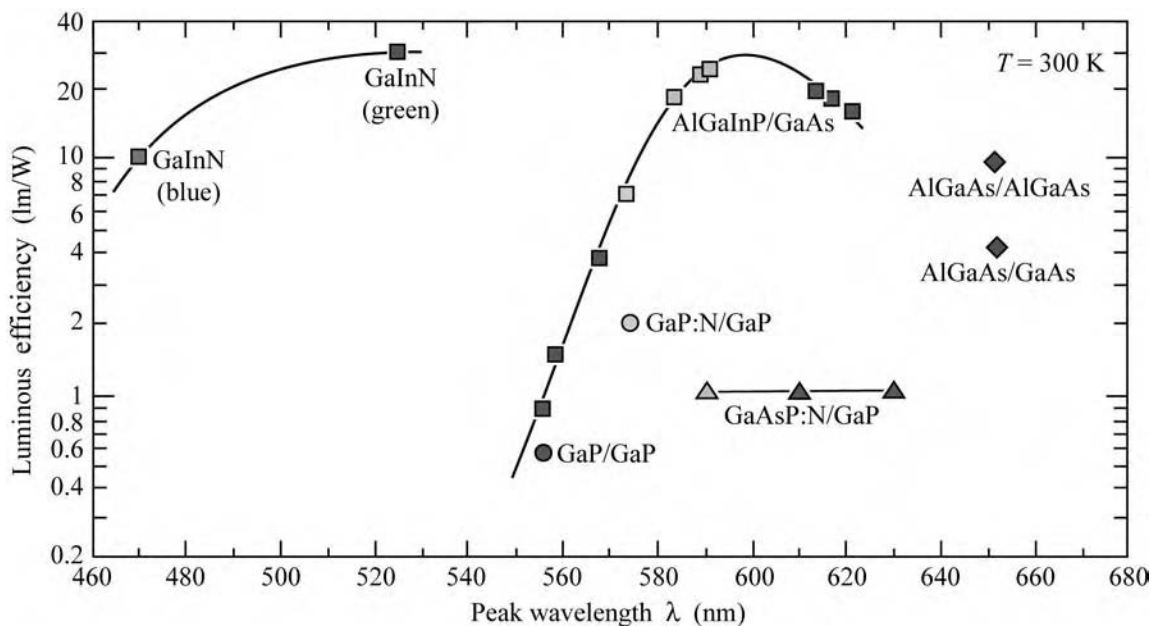


Fig. 12.14. Overview of luminous efficiency of visible LEDs made from the phosphide, arsenide, and nitride material system (adapted from United Epitaxy Corporation, 1999; updated 2000).

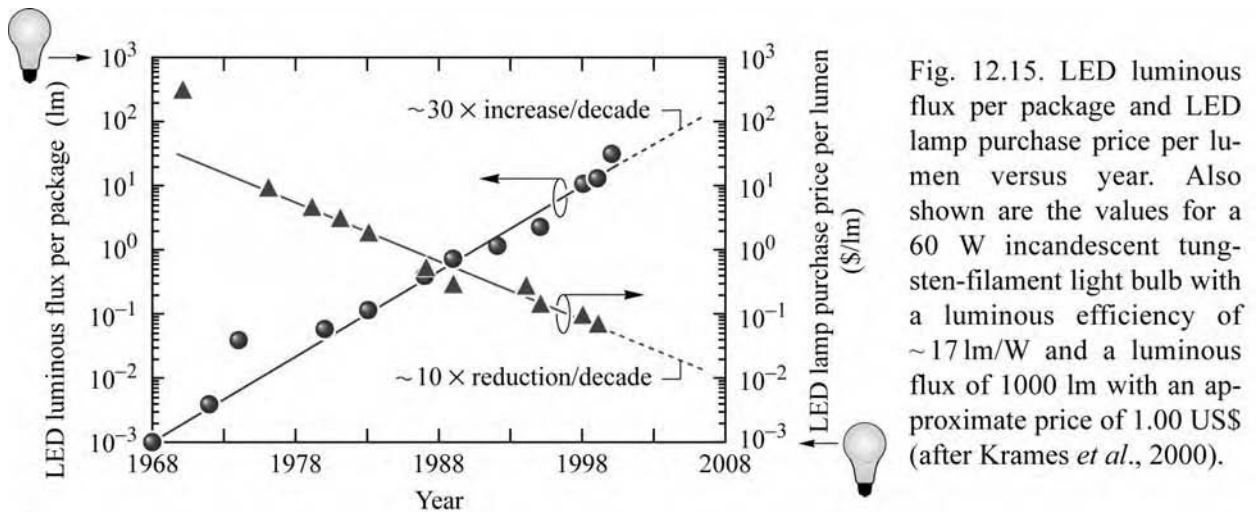
The fact that amber (dark yellow or orange–yellow) and orange AlGaInP LEDs provide an excellent luminous efficiency is also due to the high eye sensitivity in this wavelength range. Note that the maximum eye sensitivity occurs in the green at 555 nm, so that a green LED emitting at that wavelength appears brighter than an LED with the same optical power emitting at any other wavelength.

Owing to the high luminous efficiency and the lower manufacturing cost compared with green GaInN LEDs, amber AlGaInP LEDs are used in applications where high brightness and low power consumption are desirable, e.g. in highway signage applications. In the 1980s, such highway signs were made with power-hungry incandescent lamps powered by an electrical generator which, in turn, was powered by a gasoline engine. Today such signs use energy-saving amber LEDs powered by solar cells (during daytime) and batteries (at night).

Figures 12.13 and 12.14 also show low-power and low-cost LEDs such as GaAsP and GaP:N LEDs with much lower luminous efficiency. These LEDs are not suitable for high-brightness applications due to their inherently lower quantum efficiency. The GaAsP LEDs are mismatched to the GaAs substrate and therefore have a low internal efficiency. The GaP:N LEDs also have a low efficiency due to the nitrogen-impurity-assisted nature of the radiative transition.

Not only the *luminous efficiency* but also the *total power* emitted by an LED is of importance for many applications, in particular for applications where a high luminous flux is required. This

is the case, for example, in signage, traffic light, and illumination applications. Whereas conventional light sources such as incandescent light bulbs can be easily scaled up to provide high light power, individual LEDs are low-power devices. The historical development of the luminous flux per LED package, measured in lumens, is shown in Fig. 12.15 (Krames *et al.*, 2000). The figure shows that the luminous flux per LED package has increased by about four orders of magnitude over a period of 30 years.



For comparison, Fig. 12.15 shows the luminous flux and an approximate purchase price of a 60 W incandescent light bulb with a luminous flux of 1000 lm. The figure illustrates that continued progress in the performance and manufacturing cost of LEDs is required to enable LEDs to enter into the general illumination market. Note that the cost shown in the figure is just the purchase price of the lamp and does not include the cost for the electrical power consumed over the lifetime of the lamp. The cost of the electrical power required to run an incandescent light bulb is much higher than the purchase price of the lamp so that efficient light sources can have a cost advantage over incandescent lights even if the initial purchase price is much higher.

12.6 Optical characteristics of high-brightness LEDs

Optical emission spectra of red AlGaInP and green and blue GaInN LEDs are shown in Fig. 12.16 (Toyoda Gosei, 2000). Comparison of the emission spectra reveals that the green LED has a wider emission spectrum than either the blue or the red LED. This can be attributed to the well-known difficulties of growing GaInN with a high In content. It has been found that *In-rich clusters* or *quantum dots* form during the growth of GaInN, especially in GaInN with a high In

content. It is known that the formation of such In clusters depends strongly on the growth conditions.

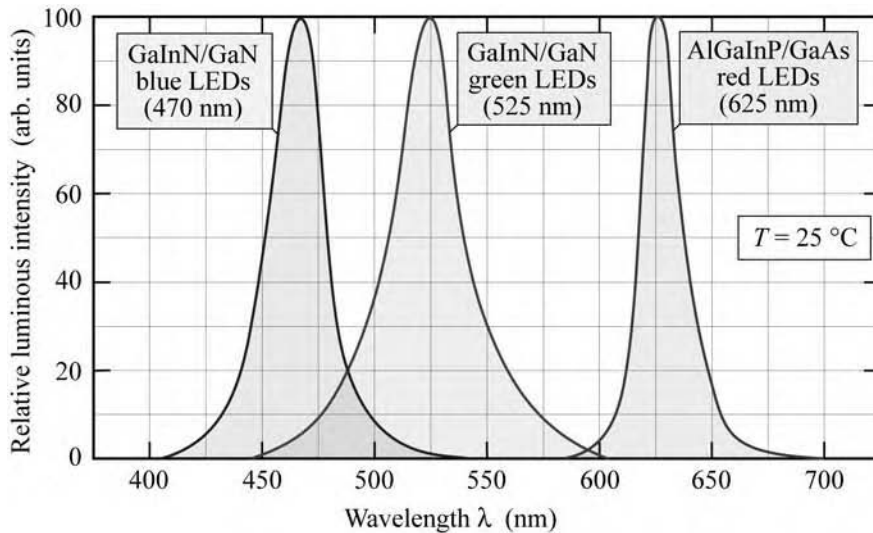


Fig. 12.16. Typical emission spectrum of GaInN/GaN blue, GaInN/GaN green, and AlGaInP/GaAs red LEDs at room temperature (after Toyoda Gosei Corp., 2000).

All LEDs shown in Fig. 12.16 have an active region composed of a *semiconductor alloy*. Alloy broadening, i.e. the broadening of the emission band due to random fluctuations of the chemical composition of the active material, will lead to spectral broadening that goes beyond the $1.8 kT$ linewidth expected for thermally broadened emission bands.

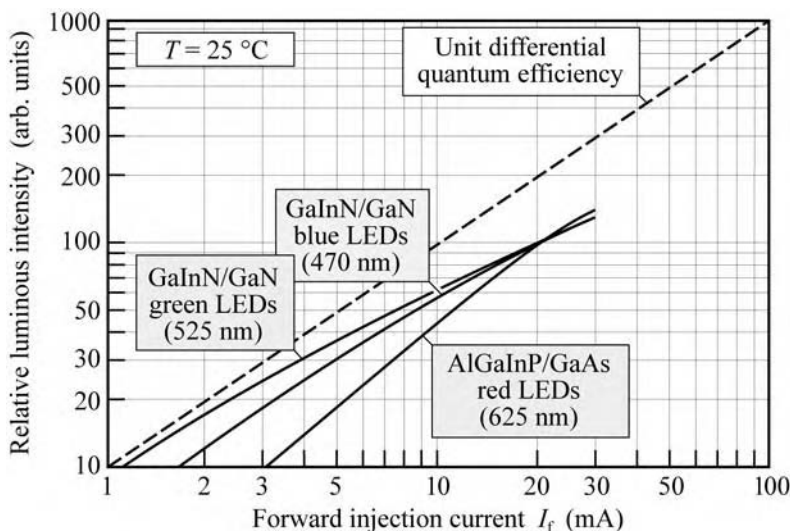


Fig. 12.17. Typical light output power vs. injection current of GaInN/GaN blue, GaInN/GaN green, and AlGaInP/GaAs red LEDs at room temperature (adopted from Toyoda Gosei Corp., 2000).

The light power versus injection current is shown in Fig. 12.17. A linear dependence with unit slope, i.e. unit differential quantum efficiency, is expected for light-versus-current curves in ideal LEDs. The unit-slope line is represented by the dashed line in Fig. 12.17. The mature

AlGaInP LED closely follows the unit-slope line. However, the green LED has a large deviation from the unit differential quantum efficiency slope due to the lower maturity of the GaInN material system, especially with high concentrations of In.

The temperature dependence of the optical emission intensity is shown in Fig. 12.18. The figure reveals that III–V nitride diodes have a much weaker temperature dependence than the AlGaInP LED. Two factors contribute to the weaker temperature dependence. Firstly, the active-to-confinement barriers are higher in the wide-gap III–V nitride material system than in other III–V material systems. Consequently, carriers in the GaInN active region are very well confined. Thus carrier leakage out of the well and carrier overflow are of little relevance in GaInN LEDs. Secondly, AlGaInP has a direct–indirect transition of the bandgap at about 555 nm. At elevated temperatures, the indirect valleys become increasingly populated so that the radiative efficiency decreases.

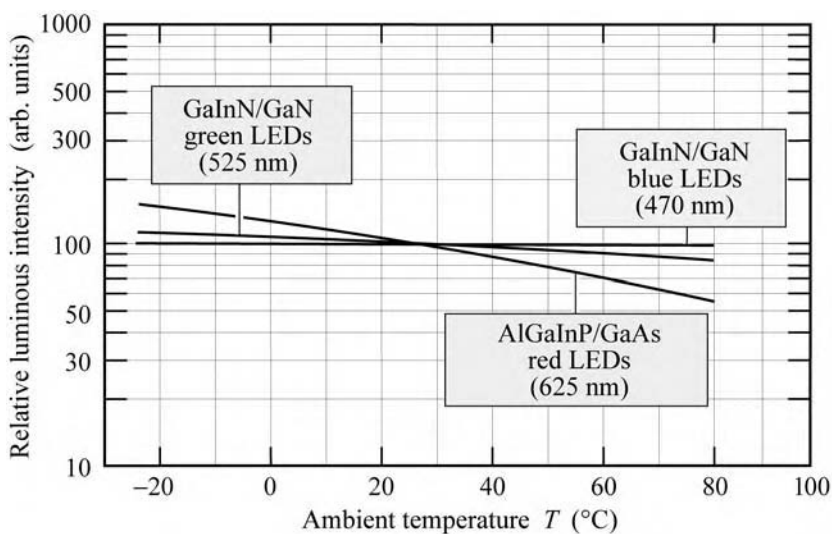


Fig. 12.18. Typical output intensity of GaInN/GaN blue, GaInN/GaN green, and AlGaInP/GaAs red LEDs versus ambient temperature (after Toyoda Gosei Corp., 2000).

12.7 Electrical characteristics of high-brightness LEDs

The forward current–voltage (I – V) characteristics of a blue GaInN, a green GaInN, and a red AlGaInP LED are shown in Fig. 12.19. The forward turn-on voltage scales with the emission energy, indicating a well-behaved characteristic. Closer inspection of the forward voltage (at 1 mA) of the green LED ($V_{f,\text{green}} = 2.65$ V) indicates that it is very similar to the blue LED ($V_{f,\text{blue}} = 2.75$ V) even though the emission energies of the blue and green LED are quite different ($\lambda_{\text{blue}} = 470$ nm, $h\nu_{\text{blue}} = 2.64$ eV; $\lambda_{\text{green}} = 525$ nm, $h\nu_{\text{green}} = 2.36$ eV). The small difference in forward voltage indicates that carriers probably lose energy by phonon emission when injected

from the GaN barrier into the GaInN active region. They lose more energy when being injected from the GaN barrier into the In-rich active region of the green LED. The energy, dissipated by emission of phonons, is supplied by the external voltage applied to the LED.

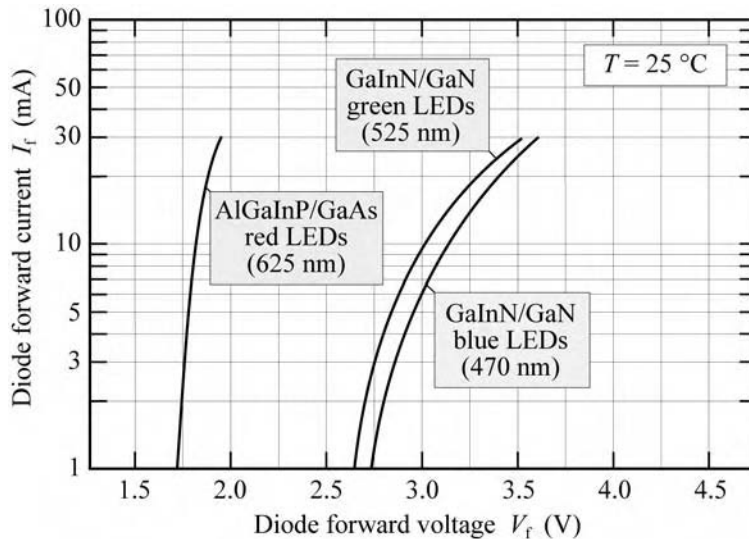


Fig. 12.19. Typical forward current–voltage (I – V) characteristic of GaInN/GaN blue, GaInN/GaN green, and AlGaInP/GaAs red LEDs at room temperature (after Toyoda Gosei Corporation, 2000).

The diode series resistance can be inferred from the slope of the I – V characteristics. The blue and green diodes have a higher series resistance than the red AlGaInP diode. The larger resistance in GaInN LEDs can be attributed to several factors including the “lateral” resistance in the n-type buffer layer for devices grown on sapphire substrates, strong polarization effects occurring in the nitride material family, lower p-type conductivity in the cladding layer, and higher p-type contact resistance. The lower p-type conductivity is due to the high acceptor activation energy (approximately 200 meV) in GaN and GaInN so that only a small fraction of acceptors is activated.

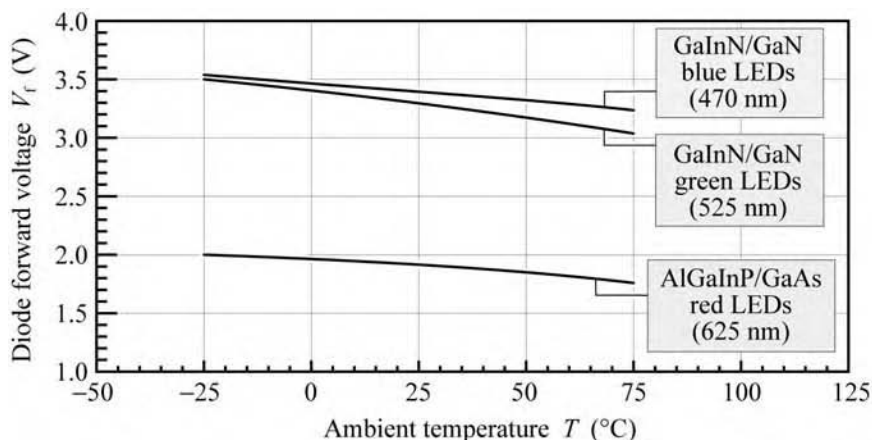


Fig. 12.20. Typical diode forward voltage at a current of 30 mA of GaInN/GaN blue, GaInN/GaN green, and AlGaInP/GaAs red LEDs versus temperature (after Toyoda Gosei Corp., 2000).

The temperature dependence of the forward voltage at a diode current of 30 mA is shown in Fig. 12.20. For all diodes shown, the forward voltage decreases as the temperature is increased. The decrease in forward voltage is due to the decrease of the bandgap energy. In the blue and green GaInN diodes, the lower forward voltage is also due to the decrease in series resistance occurring at high temperatures. This resistance decrease is due to the higher acceptor activation occurring at elevated temperatures and the resulting higher conductivity of the p-type GaN and GaInN layers.

References

- Bradley R. R., Ash R. M., Forbes N. W., Griffiths R. J. M., Jebb D. P., and Shepard H. E. "Metalorganic chemical vapor deposition of junction isolated GaAlAs/GaAs LED structures" *J. Cryst. Growth* **77**, 629 (1986)
- Campbell J. C., Holonyak Jr. N., Craford M. G., and Keune D. L. "Band structure enhancement and optimization of radiative recombination in GaAsP (and InGaP:N)" *J. Appl. Phys.* **45**, 4543 (1974)
- Casey Jr. H. C. and Panish M. B. *Heterostructure Lasers, Part A and Heterostructure Lasers, Part B* (Academic Press, San Diego, 1978)
- Chen C. H., Stockman S. A., Peanasky M. J., and Kuo C. P. "OMVPE growth of AlGaInP for high-efficiency visible light-emitting diodes" in *High Brightness Light Emitting Diodes* edited by G. B. Stringfellow and M. G. Craford, *Semiconductors and Semimetals* **48**, (Academic Press, San Diego, 1997)
- Craford M. G., Shaw R. W., Herzog A. H., and Groves W. O. "Radiative recombination mechanisms in GaAsP diodes with and without nitrogen doping" *J. Appl. Phys.* **43**, 4075 (1972)
- Craford M. G. "Overview of device issues in high-brightness light-emitting diodes" in *High Brightness Light Emitting Diodes* edited by G. B. Stringfellow and M. G. Craford, *Semiconductors and Semimetals* **48** (Academic Press, San Diego, 1997)
- Craford M. G. "The bright future of light-emitting diodes" Plenary talk on light emitting diodes at the MRS Fall Meeting, Boston Massachusetts December (1999)
- Dallessasse J. M., El-Zein N., Holonyak Jr. N., Hsieh K. C., Burnham R. D., and Dupuis R. D. "Environmental degradation of AlGaAs-GaAs quantum-well heterostructures" *J. Appl. Phys.* **68**, 2235 (1990)
- Grimmeiss H. G. and Scholz H. "Efficiency of recombination radiation in GaP" *Phys. Lett.* **8**, 233 (1964)
- Groves W. O. and Epstein A. S. "Epitaxial deposition of III-V compounds containing isoelectronic impurities" US Patent 4,001,056 (1977)
- Groves W. O., Herzog A. H., and Craford M. G. "Process for the preparation of electroluminescent III-V materials containing isoelectronic impurities" US Patent Re. 29,648 (1978a)
- Groves W. O., Herzog A. H., and Craford M. G. "GaAsP electroluminescent device doped with isoelectronic impurities" US Patent Re. 29,845 (1978b)
- Holonyak Jr. N. and Bevacqua S. F. "Coherent (visible) light emission from Ga(AsP) junctions" *Appl. Phys. Lett.* **1**, 82 (1962)
- Holonyak Jr. N., Bevacqua S. F., Bielan C. V., and Lubowski S. J. "The "direct-indirect" transition in Ga(AsP) p-n junctions," *Appl. Phys. Lett.* **3**, 47 (1963)
- Holonyak Jr. N., Nuese C. J., Sirkis M. D., and Stillman G. E., "Effect of donor impurities on the direct-indirect transition in Ga(AsP)" *Appl. Phys. Lett.* **8**, 83 (1966)
- Ishiguro H., Sawa K., Nagao S., Yamanaka H., and Koike S. "High efficient GaAlAs light emitting diodes of 660 nm with double heterostructure on a GaAlAs substrate" *Appl. Phys. Lett.* **43**, 1034 (1983)
- Ishimatsu S. and Okuno Y. "High efficiency GaAlAs LED" *Optoelectron. Dev. Technol.* **4**, 21 (1989)
- Kish F. A. and Fletcher R. M. "AlGaInP light-emitting diodes" in *High Brightness Light Emitting Diodes* edited by G. B. Stringfellow and M. G. Craford, *Semiconductors and Semimetals* **48** (Academic

- Press, San Diego, 1997)
- Krames M. R. *et al.* “High-power truncated-inverted-pyramid $(\text{Al}_x\text{Ga}_{1-x})_{0.5}\text{In}_{0.5}\text{P}/\text{GaP}$ light emitting diodes exhibiting $> 50\%$ external quantum efficiency” *Appl. Phys. Lett.* **75**, 2365 (1999)
- Krames M. R. *et al.* “High-brightness AlGaInN light emitting diodes” *Proc. SPIE* **3938**, 2 (2000)
- Krames M. R., Amano H., Brown J. J., and Heremans P. L. “High-efficiency light-emitting diodes” Special Issue of *IEEE J. Sel. Top. Quantum Electron.* **8**, 185 (2002)
- Logan R. A., White H. G., and Trumbore F. A. “P-n junctions in compensated solution grown GaP” *J. Appl. Phys.* **38**, 2500 (1967a)
- Logan R. A., White H. G., and Trumbore F. A. “P-n junctions in GaP with external electroluminescence efficiencies $\sim 2\%$ at 25°C ” *Appl. Phys. Lett.* **10**, 206 (1967b)
- Logan R. A., White H. G., and Wiegmann W. “Efficient green electroluminescent junctions in GaP” *Solid State Electron.* **14**, 55 (1971)
- Mueller G. (editor) *Electroluminescence I, Semiconductors and Semimetals* **64** (Academic Press, San Diego, 1999)
- Mueller G. (editor) *Electroluminescence II, Semiconductors and Semimetals* **65** (Academic Press, San Diego, 2000)
- Nakamura S. and Fasol G. *The Blue Laser Diode* (Springer, Berlin, 1997)
- Nishizawa J., Koike M., and Jin C. C. “Efficiency of GaAlAs heterostructure red light emitting diodes” *J. Appl. Phys.* **54**, 2807 (1983)
- Nuese C. J., Stillman G. E., Sirkis M. D., and Holonyak Jr. N., “Gallium arsenide-phosphide: crystal, diffusion, and laser properties” *Solid State Electron.* **9**, 735 (1966)
- Nuese C. J., Tietjen J. J., Gannon J. J., and Gossenberger H. F. “Optimization of electroluminescent efficiencies for vapor-grown GaAsP diodes” *J. Electrochem. Soc.: Solid State Sci.* **116**, 248 (1969)
- Pilkuhn M. and Rupprecht H. “Electroluminescence and lasing action in GaAsP” *J. Appl. Phys.* **36**, 684 (1965)
- Prins A. D., Sly J. L., Meney A. T., Dunstan D. J., O'Reilly E. P., Adams A. R., and Valster A. J. *Phys. Chem. Solids* **56**, 349 (1995)
- Steranka F. M., DeFevre D. C., Camras M. D., Tu C.-W., McElfresh D. K., Rudaz S. L., Cook L. W., and Snyder W. L. “Red AlGaAs light emitting diodes” *Hewlett-Packard Journal* p. 84 August (1988)
- Steranka F. M. “AlGaAs red light-emitting diodes” in *High Brightness Light Emitting Diodes* edited by G. B. Stringfellow and M. G. Craford, *Semiconductors and Semimetals* **48** (Academic Press, San Diego, 1997)
- Stringfellow G. B. and Craford M. G. (Editors) *High Brightness Light Emitting Diodes, Semiconductors and Semimetals* **48** (Academic Press, San Diego, 1997)
- Strite S. and Morkoc H., “GaN, AlN, and InN: A review” *J. Vac. Sci. Technol.* **B 10**, 1237 (1992)
- Tien P. K. Original version of the graph is courtesy of P. K. Tien of AT&T Bell Laboratories (1988)
- Toyoda Gosei Corporation, Japan, LED product catalog (2000)
- United Epitaxy Corporation, Taiwan, General LED and wafer product catalog (1999)
- Wolfe C. M., Nuese C. J. and Holonyak Jr. N. “Growth and dislocation structure of single-crystal Ga(AsP)” *J. Appl. Phys.* **36**, 3790 (1965)
- Wu J., Walukiewicz W., Yu K. M., Ager III J. W., Haller E. E., Lu H., Schaff W. J., Saito Y., and Nanishi Y. “Unusual properties of the fundamental bandgap of InN” *Appl. Phys. Lett.* **80**, 3967 (2002a)
- Wu J., Walukiewicz W., Yu K. M., Ager III J. W., Haller E. E., Lu H., and Schaff W. J. “Small bandgap bowing in $\text{In}_{1-x}\text{Ga}_x\text{N}$ alloys” *Appl. Phys. Lett.* **80**, 4741 (2002b)

3. Surcroissance latérale épitaxiale (ELO)

3.1. ELO standard

LEO = Lateral Epitaxy Overgrowth

La voie la plus prometteuse actuellement pour réduire les dislocations au-delà de la nucléation 3D est l'ELO, qui a été récemment développé en MOVPE [79-82], HVPE [83-84] et par sublimation (CSV). Cette méthode n'a été utilisée pour les nitrures qu'à partir de 1997, quand la durée de vie d'une diode laser bleue fabriquée sur ELO a atteint 10000 heures [85]. L'ELO repose sur deux propriétés spécifiques de la croissance en phase vapeur, à savoir l'épitaxie sélective et l'anisotropie de croissance n'est possible qu'à partir d'une phase vapeur. Cette méthode est décrite en détails dans un article de revue [86]

3.2. Problématique

L'Épitaxie Sélective correspond à la croissance contrôlée spatialement d'une couche épitaxiale dans des ouvertures réalisées dans un masque recouvrant le substrat de départ, ce masque étant un diélectrique tel que l'oxyde ou le nitrure de silicium. Il s'agit de contrôler les conditions de croissance pour avoir une sélectivité

parfaite, c'est-à-dire croissance uniquement dans les ouvertures et aucun dépôt sur le masque. Cette parfaite sélectivité est atteinte quand la sursaturation des espèces active sur le diélectrique est suffisamment basse pour éviter tout dépôt tandis la barrière à la nucléation reste suffisamment faible pour permettre le dépôt dans les ouvertures. En phase vapeur (MOVPE ou HVPE), l'absence de dépôt sur le masque est contrôlée par les paramètres de la croissance, pression, température, pression partielles des espèces actives, composition du gaz vecteur. L'épitaxie sélective de GaN/saphir a été démontrée par Kato. [87] La figure 11 illustre cette sélectivité, GaN est d'abord élaboré sur saphir, puis recouvert d'une couche de SiN (2-3 nm) sur laquelle on réalise des ouvertures ponctuelles. Lors de la reprise de croissance, la croissance ne s'effectue qu'à partir des ouvertures (croissance sélective), les ouvertures sont d'abord remplies, puis, lorsque la croissance se poursuit, la croissance latérale commence et conduit à la formation de pyramides avec des facettes latérales {1-101}. Cette technique de croissance est appelée SAE pour sélective Area Epitaxy et peut être utilisée pour d'autres applications que l'ELO, comme par exemple la fabrication de microprismes hexagonaux. [88]

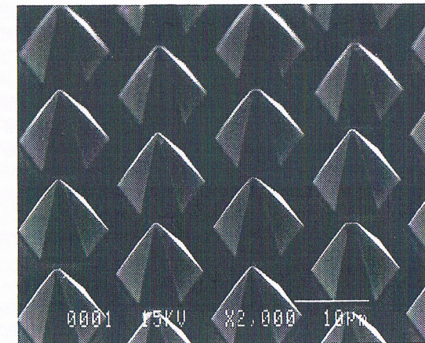


Fig. 11: Epitaxie sélective de GaN/saphir.

L'anisotropie de croissance se manifeste par des vitesses de croissance différentes pour différentes faces cristallographiques. Ceci avait été observé depuis au moins 2 décennies en HVPE. Il y a par exemple 2 ordres de grandeur de différence entre les vitesses de croissance des plans $\{111\}_{\text{Ga}}$ et $\{1-11\}_{\text{As}}$ dans GaAs. Ces faits s'expliquent très bien par l'analyse de la cinétique d'incorporation des espèces actives en surface. Une anisotropie de croissance existe aussi en MOVPE, mais reste limitée. Cette anisotropie a été quantifiée dans le cas de GaAs par la croissance sur des surfaces masquées et gravées ou sur des demi-sphères de GaAs. [89] Il se produit une anisotropie de croissance par ce que les espèces moléculaires qui diffusent en surface sont incorporées préférentiellement

sur des sites cristallographiques spécifiques. En MOVPE, les espèces actives sont apportées à l'interface de croissance avec un flux uniforme, l'incorporation à l'interface de croissances se produit après diffusion (cinétiquement contrôlée) des espèces adsorbées en surface. La MOVPE est un processus de croissance intervenant à très forte sursaturation et la vitesse de croissance est contrôlée par la diffusion des espèces actives à travers une couche limite. C'est pourquoi la vitesse de croissance sur des substrats d'orientation cristallographique différente est sensiblement la même. Par contre, l'anisotropie de croissance se manifeste seulement quand les espèces qui diffusent rencontrent différents plans cristallographiques lors de leur libre parcours moyen λ_s .

L'effet combiné de l'épitaxie sélective et de l'anisotropie de croissance ont été mis à profit pour fabriquer des structures quantiques. En ELO, après que les ouvertures aient été remplies, l'anisotropie de croissance conduit à une surcroissance épitaxiale latérale (**lateral overgrowth**). Ces surcroissances reflètent l'anisotropie de croissance et peuvent conduire à des motifs très originaux comme un laser AlGaAs/GaAs émettant à partir de 6 facettes d'une surcroissance latérale hexagonale.

De tels effets ne sont pas observés en Epitaxie par Jets Moléculaires (MBE), ce qui ne permet pas d'utiliser la technologie ELO [90].

3.3. Partie Expérimentale

La technologie ELO peut se décrire comme suit:

- on réalise d'abord la croissance d'un template GaN/saphir ou GaN/6H-SiC
- Puis sur cette couche initiale on dépose un masque diélectrique (SiO_2 or SiN) en utilisant des technologies de dépôt bien établies telles que la CVD or PECVD.
- Puis on réalise par photolithographie des ouvertures, la plupart du temps un ensemble d'ouvertures parallèles de quelques μm de large séparées de plusieurs μm selon des directions cristallographiques bien précises.

Lors de la reprise d'épitaxie, que ce soit en MOVPE [91] ou en HVPE ou encore par CSVT [92-93] il y a épitaxie sélective, plus précisément la recroissance commence dans les ouvertures sans qu'il ait nucléation sur le masque diélectrique. Dans des conditions optimisées, quand GaN ainsi épitaxié a atteint le bord du masque, la croissance latérale commence et finalement conduit à une coalescence totale et une surface lisse utilisable pour la fabrication de composants. L'idée fondamentale, lorsque l'on observe le comportement des dislocations (Fig. 12), est que cette technique filtre en quelque sorte les dislocations :

- les dislocations qui arrivent sous le masque sont arrêtées
- celles qui arrivent dans les ouvertures continuent dans GaN au-dessus du masque, il y a continuité dans la densité de défauts,
- Par contre aucune dislocation ne se propage dans GaN qui croit latéralement. Cette partie (au-dessus du masque) ne présente pas de défauts étendus.

Cette technologie ELO, dite à une étape présente donc deux zones de GaN avec des qualités différentes, au-dessus des parties masquées avec des

densités de défauts étendus réduits et au-dessus des ouvertures avec les mêmes densités de défauts que le template initial. Lorsque l'on réalise des composants sur de telles structures ELO, le composant doit être impérativement réalisé sur la partie au-dessus du masque (appelée "aile"), ce qui rend la technologie assez complexe.

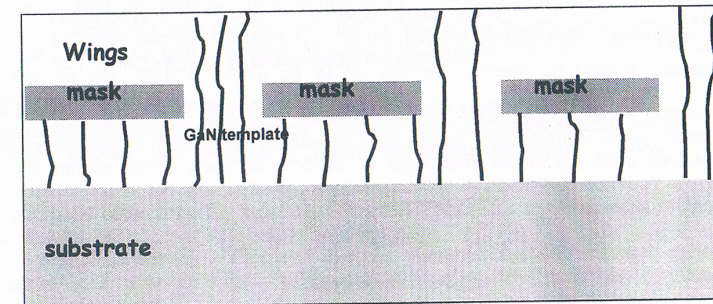
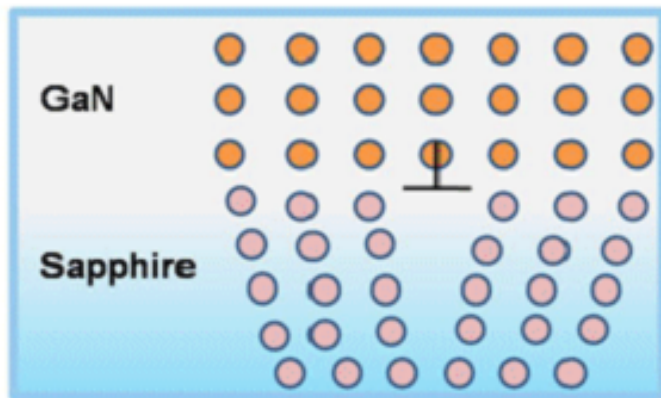


Fig. 12: Représentation schématique de l'ELO, les lignes noires représentent les dislocations traversantes.

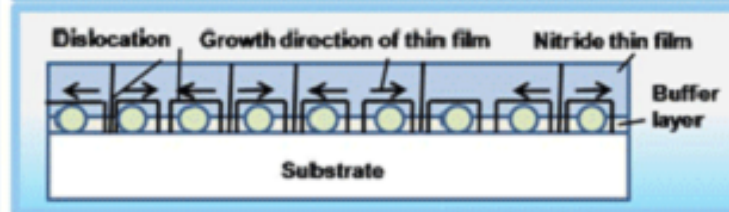
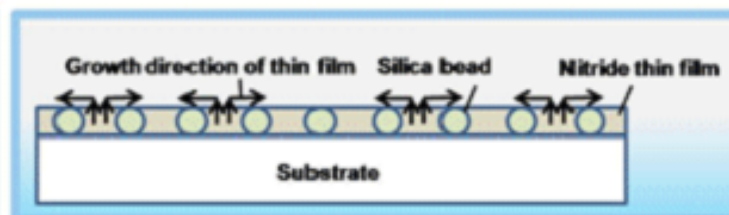
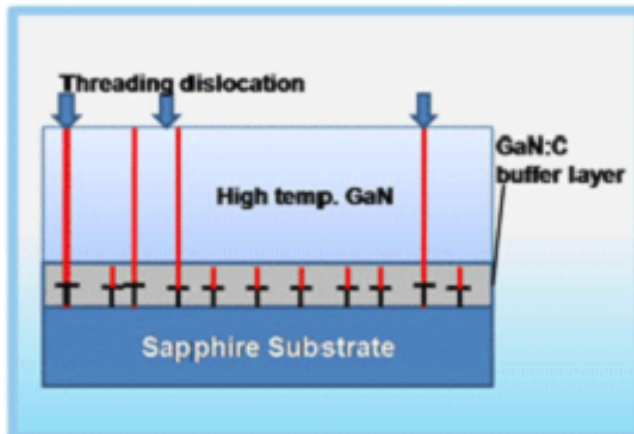
i) Reducing the threading dislocation density in nitride thin film

GaN thin film is grown on sapphire substrate. Because of lattice constant difference, high density threading dislocation is generated. To resolve this problem, we grow carbon doped GaN buffer layer before high temperature GaN growing. Another method is growing GaN thin film on the silica bead coated sapphire substrate.



	a(Å)	c(Å)	$\alpha_a (10^{-6}K^{-1})$	$\alpha_c (10^{-6}K^{-1})$
GaN	3.189	5.185	5.59	3.17
AlN	3.111	4.98	5.3	4.2
Al ₂ O ₃	4.758	12.99	7.5	8.5
InN	3.545	5.703	5.7	3.7

Lattice constant difference → high density threading dislocation generated



Mechanism of reducing threading dislocation density

Patterned substrates enhance LED light extraction

(LED MAGAZINE)

Published on: July 22, 2014

By Donggeun Ko, Jacob Yoon, and Jangho Seo

DONGGEUN KO, JACOB YOON, and JANGHO SEO describe how patterned wafers can help increase LED light extraction by reducing defect density and total internal reflection losses. Manufacturers are quickly adopting nitride-semiconductor-based LEDs as a standard light source for a wide range of products from general lighting, automobile headlights, and traffic signals to backlighting for consumer devices like HDTVs, smartphones, and tablets, and displays large and small. Still, LED performance and cost are gating broad deployment of LED technology. Indeed, lower component pricing and greater light output could boost consumer market acceptance. LED chip manufacturers are looking to patterned sapphire-substrate manufacturing techniques to maximize light extraction and overcome obstacles to broader LED usage.

Patterns applied on an LED substrate or wafer can significantly increase the light output of LEDs in two ways. The technique can increase the light emission of active quantum well layers as the result of reduced epitaxial defect density. And patterned sapphire substrates can reduce light loss due to total internal reflection (TIR) phenomena by enabling a photon scattering effect.

Researchers have developed ways to create patterns — periodic structures of varying geometry and dimension — on the sapphire substrate surface. These sapphire wafers with periodic structures of various shapes such as cone, dome, pyramid, and pillar, etc., are called patterned sapphire substrates (PSS).

Many of today's wireless platforms—especially those supported by a Bluetooth® mesh network—ensure greater flexibility and extensibility at a much lower cost than a wired system can provide.

There are two different manufacturing processes to fabricate PSS currently being practiced in the industry: dry plasma etching and wet chemical etching. Today, the majority of PSS products are produced by dry plasma etching due to its inherently effective control of precision and uniformity. The discussion of PSS fabrication in this article will focus on inductively coupled plasma (ICP) dry reactive etching (RIE).

Through work on 100-mm and 150-mm PSS with more than a dozen of the most advanced LED manufacturers, Rubicon has a unique opportunity to understand the range of requirements for effective PSS. The most critical requirements are pattern dimension, shape, and aspect ratio (i.e.,

feature height against width), and uniformity across the wafer as well as consistency from wafer to wafer.

There is no single best universal PSS recipe due to the high degree of customization of the epitaxy processes in the LED industry. Designs for patterning vary widely, and there is no convergence of PSS designs on the horizon. Typical pattern shapes include cones, domes, and square or trigonal pyramids. Although academic studies demonstrate that smaller pattern dimensions (100–1000 nm) provide greater luminous efficiency, the LED industry norm today is still 3- or 4- μm feature size.

Key process parameters contributing to these critical characteristics are the dimensional accuracy and uniformity of photoresist (PR) mask, sapphire etching selectivity against the PR mask, bias RF power, ICP process pressure, RF coil design for plasma uniformity, the ratio of trifluoromethane (CHF_3) and boron trichloride (BCl_3) gases, and substrate temperature.

Enhanced light extraction

Low light-extraction efficiency is a serious challenge for building high-brightness LEDs. Patterning on the substrate scatters a large number of photons emitted outside the TIR escape cone back into the cone, which helps more light to be extracted (Fig. 1a), creating an effect equivalent to increasing the critical angle of the escape cone (Fig. 1b). As a result, light extraction efficiency has been found to increase by as much as 30%.

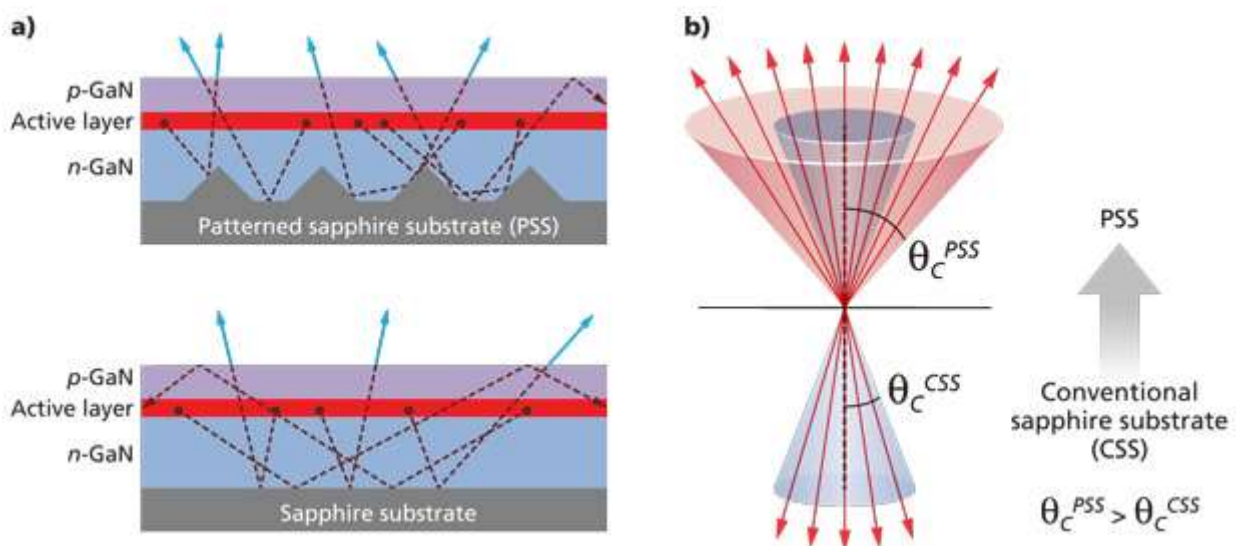


FIG. 1. PSS techniques scatter photons (a) and effectively expand the light escape cone (b), which can result in a 30% gain in light extraction efficiency.

Photons are emitted from the active quantum well layers by electron-hole recombination, and they escape the LED die into free space. In an ideal situation, all of the photons emitted by the active layers would be extracted as light output in LEDs. In reality, a large number of the emitted photons never escape the LED die for various reasons.

One key obstacle to such ideal light extraction is TIR effects due to the high refractive index of gallium nitride (GaN) versus the refractive index of free space (about 2.5 to 1.0). A large number of photons generated from the active region bounce back into the die and get trapped inside, eventually dissipating as heat. In terms of the light escape cone, defined by the critical angle of TIR, only light emitted into the escape cone exits the LED die while light emitted outside the cone gets trapped inside.

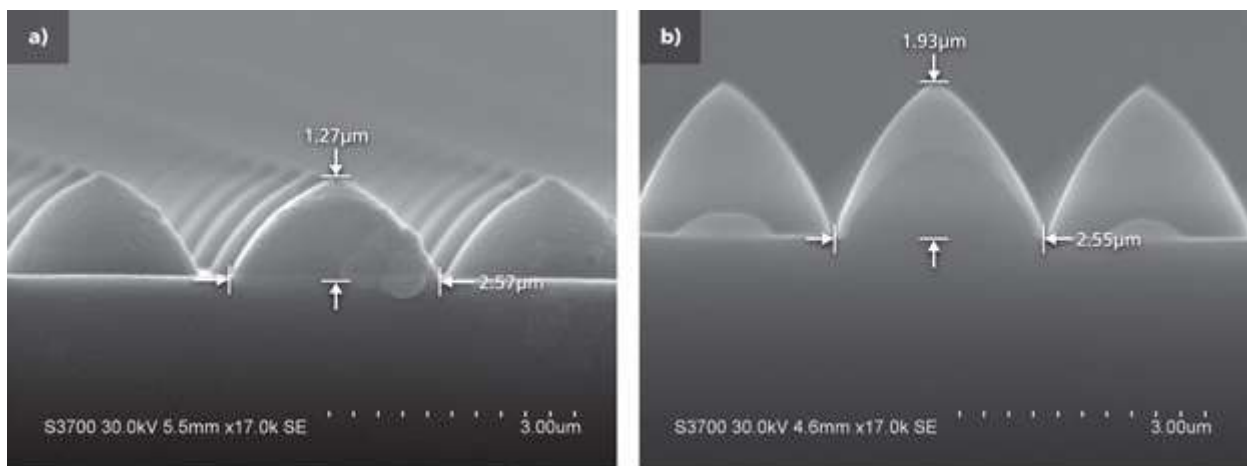


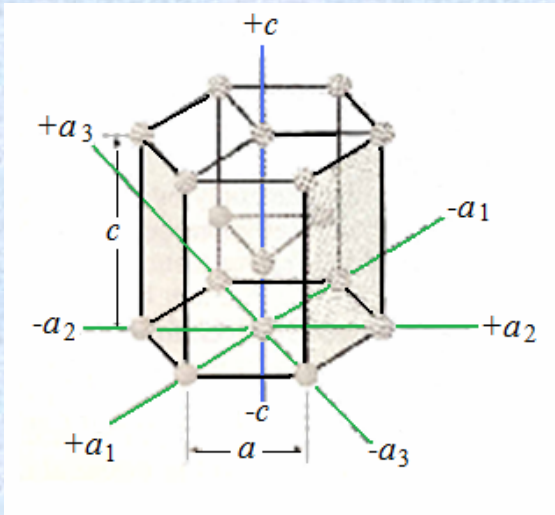
FIG. 2. PSS structures can vary. Examples include a wafer with features 1.3 μm high and 2.5 μm wide (a) and a wafer with features 1.9 μm high and 2.6 μm wide.

hexagonal structure

Miller-Bravais indices – HCP crystal plane

indices $(hkil)$ $h + k + i = 0$

three basal axes a_1, a_2, a_3 and c axis

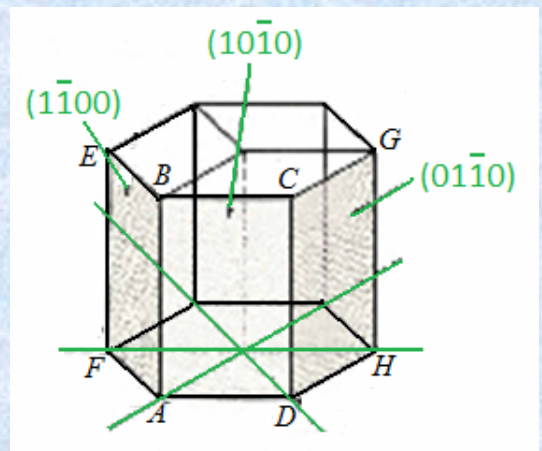
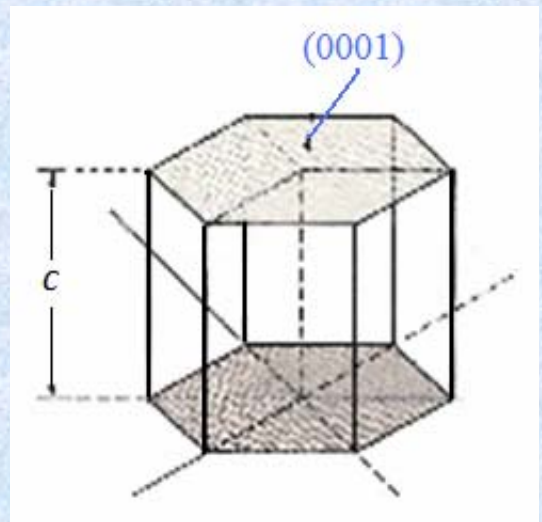


basal planes (0001)

prism planes $(ABCD)$ $(10\bar{1}0)$

$(ABEF)$ $(1\bar{1}00)$

$(CDGH)$ $(01\bar{1}0)$



The AlGaInN material system and ultraviolet emitters

13.1 The UV spectral range

The ultraviolet–visible boundary is at about 390 nm, where the 1978 CIE eye sensitivity curve has a value of 0.1% of its maximum value. This chapter concentrates on materials issues of III–V nitrides, on devices emitting in the ultraviolet (UV, $\lambda < 390$ nm), and on devices emitting in the violet near the UV–visible boundary (390–410 nm). Although the latter devices emit in the visible spectrum, they are frequently classified as UV devices. For UV devices, we will differentiate between devices having a GaInN active region ($\lambda > 360$ nm) and devices having an AlGaInN active region ($\lambda < 360$ nm).

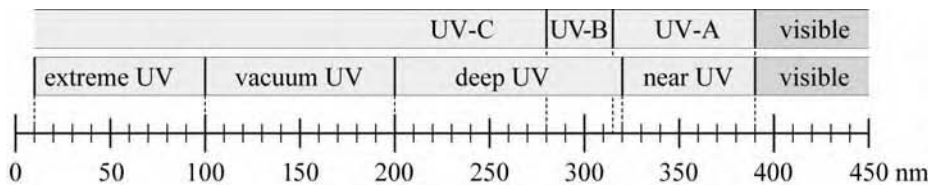
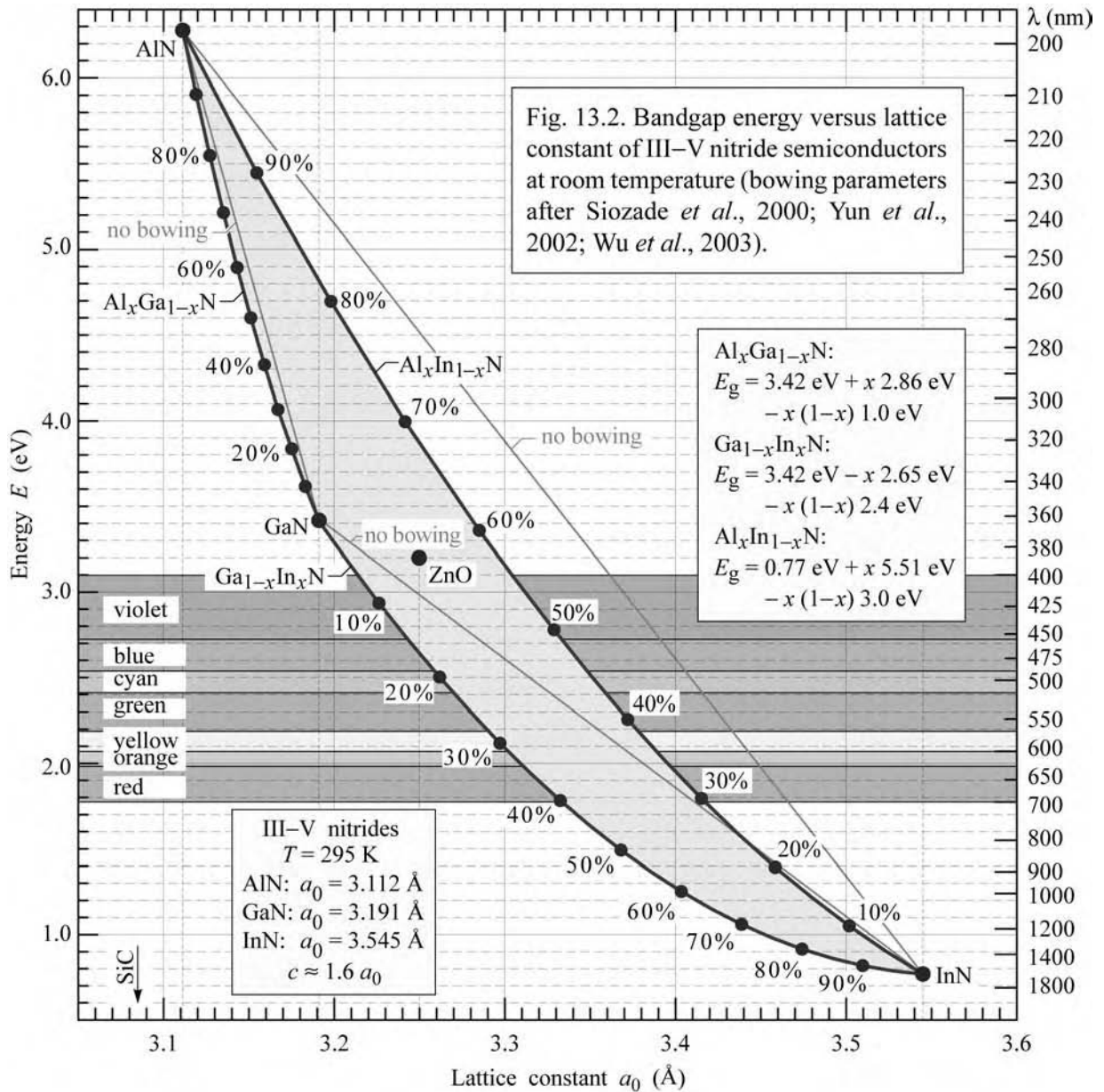


Fig. 13.1. Nomenclature of UV radiation versus wavelength (after International Congress on Light, 1932).

There are two classifications of the UV spectrum, both of which are shown in Fig. 13.1. The UV-A (315–390 nm), UV-B (280–315 nm), and UV-C (< 280 nm) classification is based on a convention established during the Second International Congress on Light in 1932 (International, 1932). UV-A radiation from the sun penetrates the earth’s atmosphere (including clouds) and, due to the high energy of UV photons, creates damage to the skin, particularly to the deeper layers of the skin. UV-A radiation also causes cataracts (the clouding of the eye’s lens), which can lead to total blindness. Both UV-B (partially absorbed by the earth’s ozone layer) and UV-C radiation (mostly absorbed by ozone layer) create serious damage to skin and eyes. Because no natural light with $\lambda \leq 280$ nm exists at the earth’s surface (i.e. in the UV-C range), this wavelength range is also referred to as the *solar-blind* range.

An alternative classification of UV radiation has evolved over time. This alternative classification has the following categories: Extreme UV (10–100 nm); vacuum UV (100–200 nm); deep UV (200–320 nm); and near UV (320–390 nm).



13.2 The AlGaInN bandgap

The bandgap energy versus lattice constant of the AlGaInN material system is shown in Fig. 13.2. The AlGaInN material system spans a very wide range of wavelengths covering the deep UV, near UV, visible, and even the near infrared spectral range. Of the three binary

semiconductors InN, GaN, and AlN, epitaxially grown GaN has been shown to be synthesizable with the highest quality. It has generally been difficult to synthesize Al-rich AlGaIn alloys and In-rich GaInN alloys with high internal quantum efficiencies.

There has been some controversy with respect to the bandgap energy of InN, which originally had been found to be about 1.9 eV. More recently, the bandgap energy was found to be much lower, namely 0.77 eV.

The energy-gap bowing can be expressed in terms of a constant, a linear term ($\propto x$) and a non-linear term [$\propto x(1-x)$] according to

$$E_g^{AB} = E_g^A + (E_g^B - E_g^A)x + x(1-x)E_b \quad (13.1)$$

with E_b called the **bowing energy** or **bowing parameter**. The bowing parameters used in Fig. 13.2 for AlGaIn, GaInN, and AlInN are based on data published by Siozade *et al.* (2000), Yun *et al.* (2002), and Wu *et al.* (2002; 2003). Recently additional data on the bowing energies have become available (Walukiewicz *et al.*, 2004).

13.3 Polarization effects in III–V nitrides

The most common epitaxial growth direction of III–V nitrides is the *c*-plane of the hexagonal wurtzite structure. III–V nitrides grown on the *c*-plane have polarization charges located at each of the two surfaces of a layer. As a result of these charges, internal electric fields occur in III–V nitrides that have a significant effect on the optical and electrical properties of this class of semiconductors.

There are **spontaneous polarization** charges as well as strain-induced or **piezoelectric polarization charges** (Bernardini *et al.*, 1997; Ambacher *et al.*, 1999; 2000; 2002). The direction of the internal electric field depends on the strain and the growth orientation (Ga face or N face) and is shown for different cases in Fig. 13.3.

The strain in the epitaxial layer can be compressive or tensile. In the compressive-strain case, the epitaxial layer of interest is laterally compressed (“laterally” meaning “in the plane of the wafer”). For example, GaInN is compressively strained when grown on a thick relaxed GaN buffer layer. In the tensile-strain case, the epitaxial layer of interest is expanded along the lateral direction. For example, AlGaIn is under tensile strain when grown on a thick relaxed GaN buffer layer.

The calculated magnitude of the electric field for common III–V nitride alloys grown on

relaxed GaN is shown in Fig. 13.4 (Gessmann *et al.*, 2002).

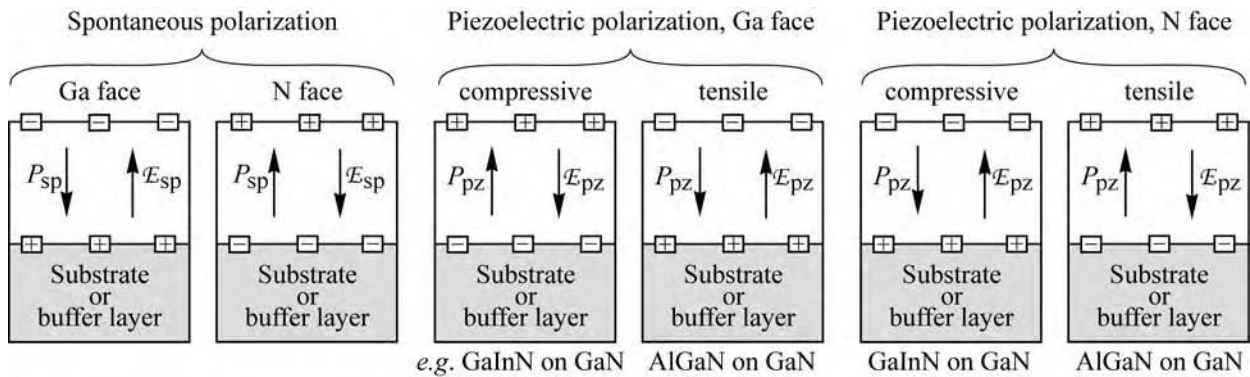


Fig. 13.3. Surface charges and direction of electric field and polarization field for spontaneous and piezoelectric polarization in III–V nitrides for Ga and N face orientation.

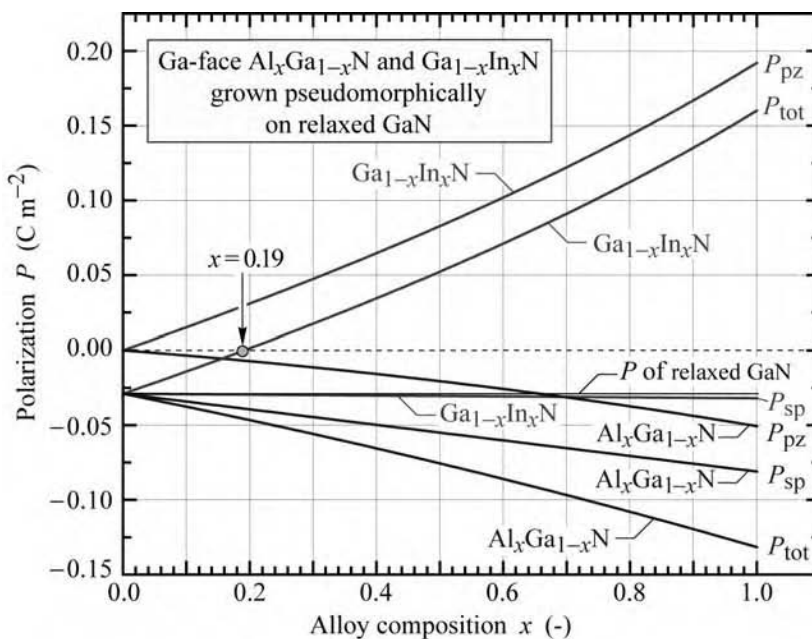


Fig. 13.4. Magnitude and direction of spontaneous and piezoelectric polarization in GaInN and AlGaIn grown pseudomorphically on relaxed GaN. Relaxed GaN has a spontaneous polarization, but no piezoelectric polarization (after Gessmann *et al.*, 2002).

A consequence of the polarization fields for quantum well structures is shown in Fig. 13.5. The quantum well layers have an internal electric field that spatially separates electrons and holes thereby preventing efficient radiative recombination. This is particularly true for thick quantum wells, *e.g.* $> 100\ \text{\AA}$. To avoid this deleterious effect, it is imperative that the quantum well layers are kept very thin. Quantum well thicknesses of $20\text{--}30\ \text{\AA}$ are typically used to minimize such electron–hole separation effects.

The large electric fields caused by the polarization effects can be screened by a high free-

carrier concentration, which can be attained through either (i) high doping of the active region or (ii) a high injection current. Screening of the internal electric field also results in a blue-shift of the emission, frequently found in GaInN LEDs as the injection current is increased.

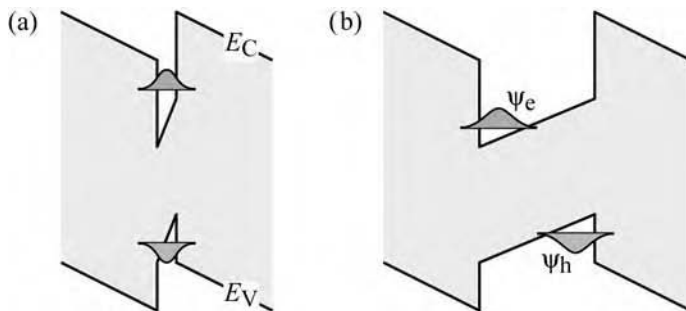


Fig. 13.5. Schematic band diagram of (a) thin and (b) thick AlGaIn/GaN active regions with polarization fields for Ga-face growth (substrate on right-hand side).

Polarization effects can be used advantageously to reduce ohmic contact resistances in GaN devices. Polarization-enhanced contacts to p-type GaN employ a thin, compressively strained GaInN cap layer that is deposited on the p-type GaN. The electric field in the GaInN cap layer is polarized in such a way that the tunneling probability of holes is enhanced (Li *et al.*, 2000; Gessmann *et al.*, 2002). Contact resistances as low as 1.1×10^{-6} and $2 \times 10^{-7} \Omega \text{cm}^2$ have been reported for non-annealed and annealed polarization-enhanced ohmic contacts to p-type GaN, respectively (Kumakura *et al.*, 2001; 2003). Both the concept of polarization-enhanced contacts and the very low specific contact resistances are remarkable because they represent a several orders-of-magnitude improvement over conventional contact technologies. The forward voltage of GaN-based LEDs with polarization-enhanced contacts is generally lower than the forward voltage of LEDs with conventional GaN contacts (Su, 2005).

13.4 Doping activation in III–V nitrides

Another problem in III–V nitrides is the low doping activation, which is caused by two effects: (i) Chemical deactivation of acceptors by hydrogen atoms bonding to the acceptors. The missing electron that acceptors strive to capture is provided by a hydrogen atom. Hydrogen is available in abundance during epitaxial growth and possible sources for hydrogen passivation include the methyl ($-\text{CH}_3$) and ethyl groups ($-\text{C}_2\text{H}_5$) of the organo-metallics, ammonia (NH_3), and hydrogen from the H_2 carrier gas. (ii) Acceptors in III–V nitrides have a high thermal activation energy which is $\gg kT$ at 300 K. As a result, only a small percentage of acceptors are ionized at room temperature.

Exercise: Activation of Mg acceptors in GaN. Mg acceptors in GaN have an activation energy of $E_a = 200$ meV. (a) Calculate the fraction of acceptors that are ionized at 300 K for an acceptor concentration of $N_{\text{Mg}} = 10^{18} \text{ cm}^{-3}$ using the formula $p = (g^{-1} N_{\text{Mg}} N_v)^{1/2} \exp(-E_a/2kT)$ where g is the acceptor ground state degeneracy ($g = 4$) and N_v is the effective density of states at the valence band edge of GaN. (b) What would be the activation of acceptors if a hydrogen atom were bonded to each acceptor?

Solution: (a) Using the formula given above, one obtains that only about 6% of the acceptors are ionized. (b) If acceptors are passivated, p-type conductivity cannot be established.

Amano *et al.* (1989) discovered that acceptor dopants can be activated by low-energy electron-beam irradiation (LEEBI). Nakamura *et al.* (1991; 1992) showed that acceptors can be activated by LEEBI as well as by thermal annealing, with thermal annealing being the preferred method. Typical annealing conditions for MOCVD-grown p-type GaN are 675–725 °C for 5 minutes in an N_2 atmosphere; p-type $\text{Al}_{0.30}\text{Ga}_{0.70}\text{N}$ is annealed at higher temperatures, typically at 850 °C for 1–2 minutes. It is believed that during thermal annealing the relatively weak acceptor–hydrogen bond is broken and that the hydrogen atoms are driven out of the epitaxial film. Hydrogen atoms are small and generally diffuse easily through the interstitial sites of a crystalline material. The heating caused by LEEBI is believed to have a similar effect.

The doping of AlGaN/GaN and AlGaN/AlGaN superlattices (rather than GaN or AlGaN bulk material) was postulated to strongly increase the electrical activation of deep acceptors such as Mg (Schubert *et al.*, 1996). Experimental increases in conductivity by a factor of 10 and more have indeed been reported by several research groups (Goepfert *et al.*, 1999, 2000; Kozodoy *et al.* 1999a, b; Kipshidze *et al.*, 2002, 2003). Figure 13.6 summarizes the problems and solutions to the doping activation in GaN and AlGaN.

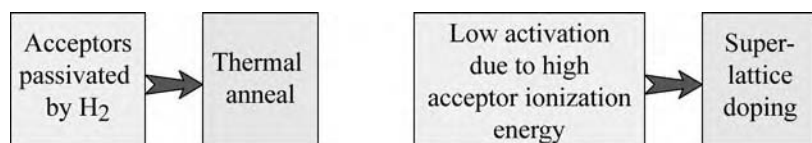


Fig. 13.6. Specific problems of p-type doping in GaN and their solution.

13.5 Dislocations in III–V nitrides

The most common substrate for GaN epitaxial growth, sapphire, is a very stable substrate in terms of its thermal, chemical, and mechanical properties. However, sapphire has the complex *corundum structure* whereas III–V nitrides crystallize in the *wurtzite structure*. Furthermore, the lattice constants of sapphire and GaN are different. As a result, GaN epitaxial films have misfit dislocations (threading and edge dislocations) that are typically on the order of 10^8 –

10^9 cm^{-2} .

The initial stages of GaN growth on sapphire are shown schematically in Fig. 13.7 (Nakamura and Fasol, 1997). The initial layer (called the faulted zone), grown at low temperatures ($\sim 500^\circ\text{C}$) and subsequently annealed, is highly dislocated. However, dislocations undergo self-annihilation during anneal, so that subsequent layers (called the semi-sound zone and the sound zone) have much lower dislocation densities. A thorough review of the initial stages of GaN epitaxial growth on sapphire and an analysis of these initial stages using atomic-force microscopy and optical reflectometry was published by Koleske *et al.* (2004).

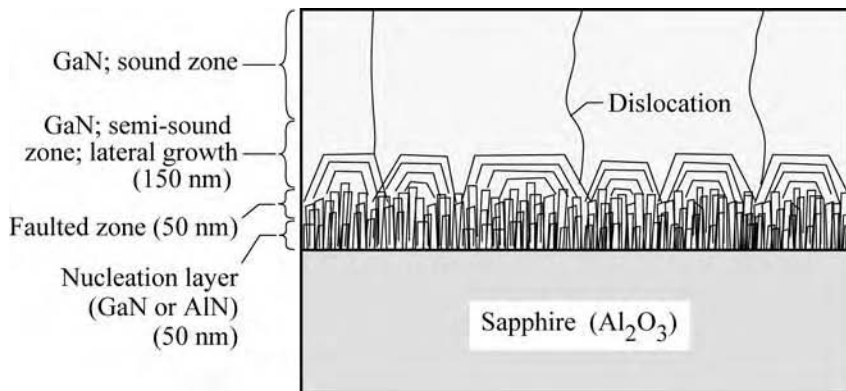


Fig. 13.7. Dislocation structure of a GaN epitaxial layer grown on sapphire by means of the GaN or AlN nucleation layer developed by Amano *et al.* (1986). The nucleation layer is normally grown at 500°C , much lower than the following GaN epitaxial layers (after Nakamura and Fasol, 1997).

Generally, dislocation lines are electrically charged so that the region surrounding a dislocation line is either coulombically attractive or repulsive to a free carrier. The nature of the coulombic interaction (attractive or repulsive) depends on the polarity of the dislocation line and the polarity of the carrier. As an example, Fig. 13.8 shows a negatively charged dislocation line which is attractive to holes and repulsive to electrons.

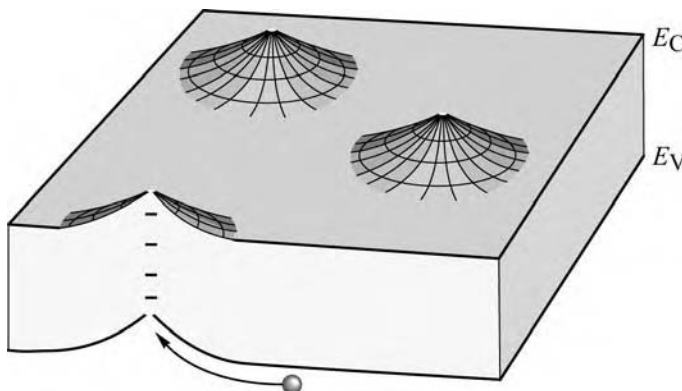


Fig. 13.8. Band diagram of semiconductor having negatively charged dislocations. Holes are attracted to dislocation lines where they must ultimately recombine with electrons.

Figure 13.9 shows the temporal development of the carrier dynamics of a positively charged

dislocation line. Initially, electrons are attracted but holes are repelled due to the potential created by the dislocation. However, the continued collection of electrons will screen the dislocation potential thereby reducing the repulsive barrier for holes. As a result, electrons and holes will recombine non-radiatively via electron states of the dislocation line. In Fig. 13.9, the electronic states of the dislocation are located within the bandgap.

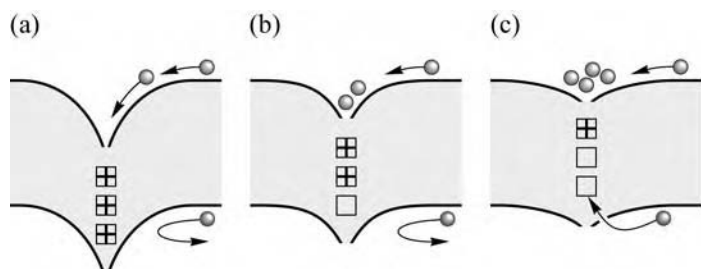


Fig. 13.9. Recombination in a positively charged dislocation. (a)–(c) Sequence shows electrons accumulating in the potential minimum thereby screening the dislocation potential and allowing holes to recombine.

A puzzling question is as to why the radiative recombination efficiency in III–V nitrides is so high despite the high density of dislocations? Several possible explanations are discussed below. However, none of these explanations has gained general acceptance.

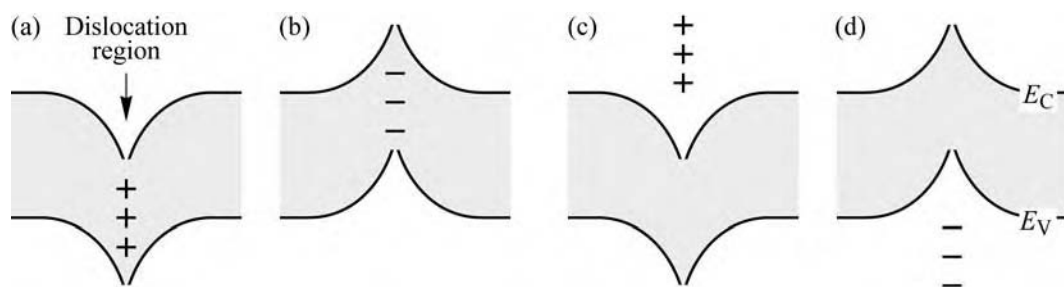


Fig. 13.10. Band diagram of dislocation: (a) donor states in gap, (b) acceptor states in gap, (c) donor states in conduction band, and (d) acceptor states in valence band. Whereas (a) and (b) lead to non-radiative recombination, (c) and (d) no not.

One possible explanation for high radiative rates in III–V nitrides is that the electronic states of the dislocation lie *outside* the forbidden gap, i.e. within the allowed bands of the semiconductor, as shown in Fig. 13.10 (c) and (d). This explanation is not in conflict with dark regions surrounding dislocations, observed in cathodoluminescence experiments (Rosner *et al.*, 1997; Albrecht *et al.*, 2002). Such dark regions unequivocally show the *absence* of radiative recombination but do not necessarily prove the *presence* of non-radiative recombination. The dark regions observed in cathodoluminescence could be explained by the incomplete screening of the dislocation potential, which would result in the repulsion of either electrons or holes, and

thus result in the absence of radiative recombination.

Other possible explanations for high radiative rates in III–V nitrides are the compositional alloy fluctuations, alloy clustering effects, and phase separation effects that necessarily result in a variation of the bandgap energy and lead to local potential minima, which carriers are attracted to and could be confined to (Nakamura and Fasol, 1997; Chichibu *et al.*, 1996; Narukawa *et al.*, 1997a, b). This explanation would be particularly suitable for ternary and quaternary alloy semiconductors such as GaInN and AlGaInN. The potential minima attract and confine carriers and prevent them from diffusing towards the dislocation lines. A band diagram showing energy-gap fluctuations and *carrier localization* is schematically illustrated in Fig. 13.11.

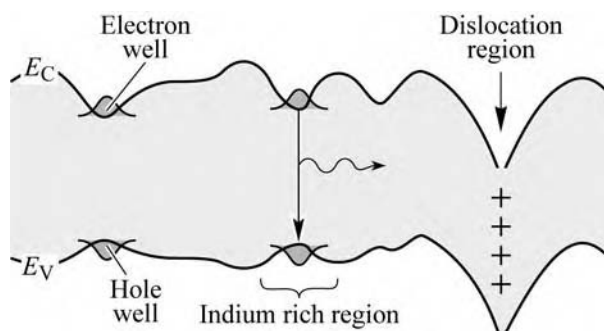


Fig. 13.11. Band diagram of GaInN having clusters of In rich regions which spatially localize carriers and prevent them from diffusing to dislocations.

Because the direct detection of indium-composition fluctuations in GaInN by transmission-electron microscopy was shown to be difficult and even ambiguous due to high-energy electron-beam induced damage, the magnitude of the indium fluctuations in GaInN is still under discussion (Smeeton *et al.*, 2003).

Recently, Hangleiter *et al.* (2005) pointed out that a reduction of GaInN/GaN quantum-well thickness occurs in the vicinity of V-shaped defects of III–V nitride epitaxial layers. The authors proposed that the higher bandgap energy associated with the thinner GaInN quantum wells shields the dislocation line-defect from mobile carriers located in the thicker (planar) GaInN quantum wells. As a result, a high radiative efficiency would be maintained in quantum-well structures despite the presence of dislocation line-defects. However, this model cannot explain the high radiative efficiency of GaN thin films.

Although a generally accepted explanation has not yet been established, it remains a fact that the radiative efficiency in III–V nitrides, in particular GaInN/GaN blue emitters, exhibits low sensitivity to the presence of dislocations. That is, high radiative efficiencies are obtained in GaInN/GaN blue emitters despite high dislocation densities. This is illustrated in Fig. 13.12 which compares the normalized efficiency of different III–V semiconductors as a function of the

dislocation density in GaAs, AlGaAs, GaP, and GaAsP. Lester *et al.* (1995) estimated a 4% radiative efficiency for GaN with a dislocation density of 10^{10} cm^{-2} . The shaded region is the estimation of the author of this book based on blue GaInN/GaN emitters. The data shown in the figure elucidate that III–V nitrides have a much higher tolerance towards dislocations as compared to III–V arsenides and phosphides.

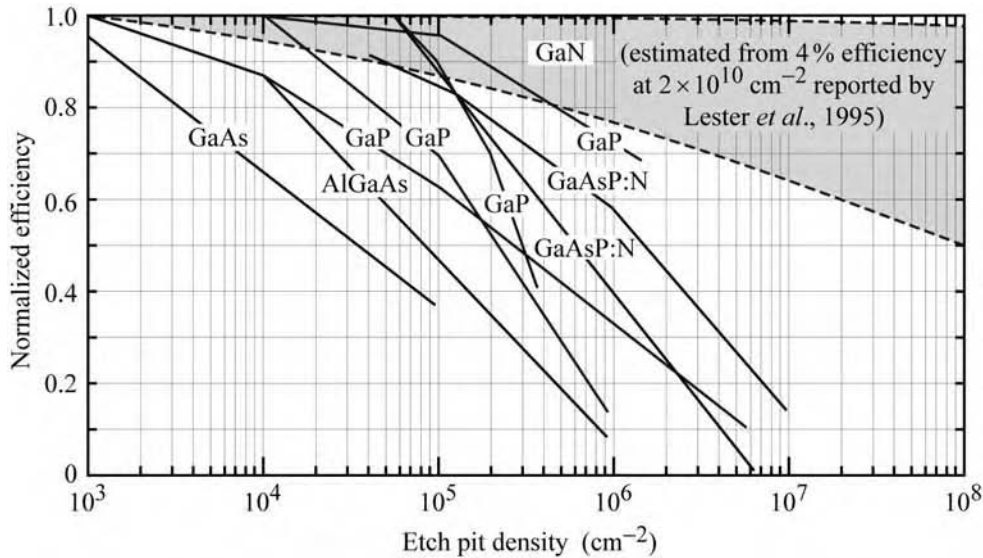


Fig. 13.12. Dependence of radiative efficiency on etch pit density (III–V arsenide and phosphide data adopted from Lester *et al.*, 1995; III–V nitride data estimated by the author of this book based on data published by Lester *et al.*, 1995).